Communications Earth & Environment https://doi.org/10.1038/s43247-026-03614-9

Article in Press

Biochar-based composite drives sulfadiazine sequestration and mitigates active resistome risks

Received: 20 December 2025

Accepted: 30 April 2026

Cite this article as: Mei, Z., Wang, F., Balcazar, J.L. *et al.* Biochar-based composite drives sulfadiazine sequestration and mitigates active resistome risks. *Commun Earth Environ* (2026). https://doi.org/10.1038/s43247-026-03614-9

Zhi Mei, Fang Wang, Jose Luis Balcazar, Chao He, Maoyuan Liao, Kelvin Sze-Yin Leung, Yuhao Fu, Syed A. Hashsham, Xin Jiang, Zhongjun Jia, Tong Zhang, James M. Tiedje & Wulf Amelung

Biochar-based composite drives sulfadiazine sequestration and mitigates active resistome risks

*Zhi Mei [1, 2, 3, 4], Fang Wang [1, 3, 5] *, Jose Luis Balcazar [2], Chao He [1,6], Maoyuan Liao [1, 3], Kelvin Sze-Yin Leung [7], Yuhao Fu [1, 3], Syed A. Hashsham [8], Xin Jiang [1, 3], Zhongjun Jia [1,9], Tong Zhang [10], James M. Tiedje [8], Wulf Amelung [4, 11]*

[1] State Key Laboratory of Soil & Sustainable Agriculture, Institute of Soil Science, Chinese Academy of Sciences, Nanjing 211135, China

[2] Catalan Institute for Water Research (ICRA-CERCA), Girona 17003, Spain

[3] University of Chinese Academy of Sciences, Beijing 100049, China

[4] Institute of Crop Science and Resource Conservation (INRES)-Soil Science and Soil Ecology, University of Bonn, Bonn 53115, Germany

[5] Joint FAO/IAEA Centre of Nuclear Techniques in Food and Agriculture, International Atomic Energy Agency, Vienna 1400, Austria

[6] Institute of Comprehensive Utilization of Resources, Kunming Metallurgical Research Institute Co., Ltd., Kunming 650021, China

[7] Department of Chemistry, Hong Kong Baptist University, Kowloon Tong, Hong Kong, China

[8] Department of Civil and Environmental Engineering, Michigan State University, East Lansing, MI 48824, USA

[9] State Key Laboratory of Black Soils Conservation and Utilization, Northeast Institute of Geography and Agroecology, Chinese Academy of Sciences, Changchun 130022, China

[10] Environmental Microbiome Engineering and Biotechnology Laboratory, Department of Civil Engineering, The University of Hong Kong, Hong Kong, China

[11] Agrosphere Institute (IBG-3), Forschungszentrum Jülich GmbH, Jülich 52428, Germany

[*] Corresponding author: Prof. Dr. Fang Wang

Address: Joint FAO/IAEA Centre of Nuclear Techniques in Food and Agriculture, International Atomic Energy Agency, 1400 Vienna, Austria

E-Mail: wangfang@issas.ac.cn, f.wang@iaea.org

Abstract

Soils are major reservoirs of antimicrobial resistance genes. Understanding how remediation strategies influence the specific bacteria responsible for antibiotic degradation remains both critical and challenging. Here, we use DNA stable-isotope probing to identify the active sulfadiazine-degrading microbiome and show that a biochar-biofilm composite carrying *Arthrobacter* D2 modulates resistance dynamics. In a less fertile Ultisol, the composite accelerated the removal of extractable sulfadiazine from bulk soil and reduced the total abundance of antimicrobial resistance genes and virulence factors. The more fertile Mollisol showed overall community resilience; however, targeted analysis of active sulfadiazine degraders revealed reduced diversity of resistance determinants in both soils. Importantly, distinguishing active sulfadiazine degraders from the total community uncovered resistance dynamics that bulk soil analyses failed to detect. These findings demonstrate that biochar-biofilm strategies can suppress resistance potential among key antibiotic-degrading bacteria, thereby potentially enhancing ecosystem safety in low-fertility soils.

Introduction

In recent years, the use of antibiotics in human medicine and livestock production has increased substantially [1]. However, a large fraction of administered antibiotics is not fully metabolized and is excreted via urine and feces into the environment [2], particularly into soils [3]. Once in soil, these compounds can promote the emergence and spread of antimicrobial resistance genes (ARGs) [4,5], which represent a major global health concern [6,7]. Importantly, antibiotics differ markedly in their ability to exert selection pressure in soils. While some antibiotics, such as β-lactams, degrade within hours and therefore have limited long-term effects on soil microbial communities [8], others, such as fluoroquinolones, are more persistent but bind strongly to soil constituents, resulting in low bioavailability and reduced biological activity [9]. In contrast, antibiotics with moderate binding affinity and environmental persistence, including sulfonamides, have been consistently associated with the emergence and spread of ARGs [10-12].

Sulfonamides are widely used in both human and veterinary medicine and are frequently detected in livestock manures and manure-amended soils at environmentally relevant concentrations (up to 1,060 μg kg^{-1}) [13]. Among them, sulfadiazine is a representative compound. It exhibits moderate environmental persistence [14,15], is commonly detected in manure and soils [16,17], and is known to exert selective pressure on microbial communities, thereby promoting the enrichment of ARGs and mobile genetic elements (MGEs) [18]. Promoting sulfadiazine dissipation may reduce antibiotic exposure and, consequently, selection pressure. However, such selection is expected primarily when sulfadiazine dissipation is driven by microbial metabolism that confers a fitness advantage to sulfadiazine degraders and/or is genetically linked to ARGs and MGEs [19]. In contrast, if sulfadiazine dissipation is dominated by sequestration processes (e.g., sequestration into non-bioavailable solid-phase matrices), the enrichment of sulfadiazine degraders and their associated ARGs may be attenuated, as bioavailable sulfadiazine concentrations would decline. These active sulfadiazine degraders can be specifically identified using ^{13}C-labeled sulfadiazine, as the incorporation of the labeled carbon into microbial DNA enables their detection through DNA stable isotope probing (DNA-SIP) [20].

One approach to reduce the concentration of bioavailable sulfadiazine is the use of biochar, which has a high adsorption capacity, a porous structure, and surface properties that facilitate sulfadiazine

sequestration while providing a suitable matrix for microbial colonization and biofilm formation [21]. Here, we inoculated biochar with *Arthrobacter* strain D2, a biofilm-forming bacterium known to enhance pollutant biodegradation [22] and with the potential to degrade antibiotics such as sulfadiazine. However, research on biochar-biofilm composites for antibiotic degradation remains limited, and their effects on the soil resistome and pathobiome are largely unknown.

This study aimed to determine whether promoting sulfadiazine degradation could serve as a strategy to mitigate the spread of ARGs. We hypothesized that biochar-biofilm composites harboring *Arthrobacter* sp. D2 would accelerate degradation and alleviate selective pressure, thereby reducing the dissemination potential of ARGs within the active microbiome. We selected an Ultisol and a Mollisol as contrasting agricultural soils that differ significantly in fertility, organic matter content, and microbial biomass, factors known to influence antibiotic sorption, partitioning, and biodegradation [23,24]. By applying ^{13}C-labeled sulfadiazine to these soils and employing DNA-SIP coupled with metagenomics, we demonstrate that the biochar composite significantly enhances degradation and reduces the proliferation of ARGs and potential pathogens in the less fertile Ultisol. In contrast, the more fertile Mollisol exhibits intrinsic ecosystem resilience, with comparatively limited responses to the treatment. These findings highlight that biochar-biofilm composites can mitigate resistance risks, particularly in soils with lower native fertility.

Results and Discussion

Fate of ^{13}C-labeled sulfadiazine, mass balance, and the sorptive sink effect

In the Mollisol, sulfadiazine dissipation was rapid, with ~9% and ~5% of the initially applied extractable ^{13}C-sulfadiazine remaining after 7 and 14 days, respectively. In contrast, dissipation was slower and more variable in the Ultisol, with ~55% remaining after 7 days and 4–24% after 14 days (Fig. 1A, D). Consequently, the less fertile Ultisol retained a larger extractable fraction after one week, indicating a longer potential exposure window.

Due to the rapid dissipation of sulfadiazine in the Mollisol, amendment with the biochar-biofilm composite did not further accelerate the depletion of bulk-soil extractable parent sulfadiazine; instead, sulfadiazine dissipation decreased by ~17% on average. In the Ultisol, the composite increased

sulfadiazine dissipation by 31 ± 6.3%, with the strongest effect observed at day 7, when bulk-soil extractable sulfadiazine declined to ~24% of the applied amount (Fig. 1A, D). After 21 days, residual sulfadiazine was < 6% of the initial level across all treatments (Fig. 1D). This counter-intuitive pattern likely arises from a preferential sulfadiazine sequestration by the composite (Fig. 1E), which reduced the remaining extractable and thus potentially bioavailable fraction of sulfadiazine in the Ultisol, where other sulfadiazine degraders were less abundant.

Compartment-level quantification of extractable parent ^{13}C-sulfadiazine in bulk soil and the recovered biofilm fraction (obtained by manual sorting) demonstrated strong partitioning into the biochar-biofilm composite (Fig. 1D–E). The biofilm-associated parent pool declined from day 14 to day 21 (Fig. 1D), indicating that this partitioned pool is dynamic rather than permanently immobilized. Consistently, extractable parent sulfadiazine concentrations were substantially higher in the recovered biofilm fraction than in bulk soil (Fig. 1E): 132-fold (day 14) and 106-fold (day 21) in the Ultisol, and 50-fold (day 14) and 46-fold (day 21) in the Mollisol. Because these values represent compartment-specific concentration enrichments (mg kg^{-1}), they primarily reflect preferential sorption and partitioning into the biochar–biofilm composite. Although transient accumulation within the biofilm microenvironment prior to transformation cannot be completely be excluded, we thus interpret this enrichment as evidence of a 'sorptive sink or partitioned pool' of extractable parent sulfadiazine rather than of a biological ^{13}C-enrichment in potential sulfadiazine degraders.

To track the redistribution and fate of ^{13}C-sulfadiazine, we established a compartment-level ^{13}C mass balance of the initially spiked ^{13}C-sulfadiazine (Fig. 1D), partitioning the tracer into (i) bulk-soil extractable parent sulfadiazine, (ii) extractable parent sulfadiazine in the recovered biofilm fraction (biofilm-associated parent sulfadiazine), (iii) cumulative $^{13}CO_2$ (a lower-bound estimate of complete mineralization), and (iv) unrecovered ^{13}C, calculated by difference and potentially comprising transformation products, bound residues, and biomass incorporation. Because the unrecovered ^{13}C pool is operationally defined by difference, it may reflect both physical sequestration/non-extractable residue formation and biotic transformation or biomass incorporation; accordingly, the present mass-balance approach cannot distinguish among these pathways. In biofilm-amended treatments, biofilm-associated parent sulfadiazine accounted for 11.9–15.4% of the initial spike on day 14, decreasing to

3.8–5.6% by day 21 (Fig. 1D). Relative to bulk-soil depletion, this corresponds to ~12–16% (day 14) and ~4–6% (day 21), whereas cumulative $^{13}CO_2$ remained < 2% of the initial spike. Most of the ^{13}C was assigned to the unrecovered pool, indicating substantial retention in non-CO_2 forms beyond reversible partitioning and complete mineralization, although the relative contributions of physical sequestration and biotic transformation could not be resolved (Fig. 1D). Therefore, the apparent acceleration of sulfadiazine dissipation with the biochar composite amendment in the Ultisol primarily reflects enhanced depletion of the bulk-soil extractable parent sulfadiazine pool via redistribution and partitioning into the extractable biofilm-associated parent sulfadiazine fraction and/or unrecovered ^{13}C pools, rather than merely reversible sorption at biochar surfaces or extensive mineralization. Because non-extractable residues can be effectively irreversible and are often poorly bioavailable, as suggested by modelling for sulfadiazine [25] and supported experimentally for difloxacin [9], it seems reasonable to infer that the biochar composite reduced the effective availability of the remaining sulfadiazine in the Ultisol, although the exact identity, stability, and remobilization potential of the unrecovered ^{13}C pools remain unresolved.

Consistently, the fraction of CO_2 efflux derived from ^{13}C-sulfadiazine increased from week 1 to week 3 in Mollisol (3.1‰ to 5.6‰) but declined in Ultisol following composite amendment (3.39‰ to 1.13‰; Fig. 1F). Nevertheless, cumulative ^{13}C-sulfadiazine mineralization remained < 2% in both soils (Fig. 1G), indicating that >98% of the added ^{13}C persisted as non-CO_2 pools (parent, transformation products, and/or bound residues) consistent with the mass balance (Fig. 1D). Hence, the observed loss of bulk-soil extractable parent sulfadiazine was mainly due to its recovery as extractable parent sulfadiazine in the recovered biofilm fraction and/or its transfer into unrecovered ^{13}C pools, which may reflect a combination of transformation, biomass incorporation, bound-residue formation and/or physical sequestration, with only a minor contribution from mineralization.

Building on these mass balance results, the enhanced depletion of extractable parent sulfadiazine in the Ultisol is most consistent with a reduction in potentially bioavailable antibiotic exposure and associated selection pressure within the sulfadiazine degraders fraction. This pattern is consistent with a combination of (i) partial transformation of parent sulfadiazine within biofilms, including co-metabolic conversion stimulated by biochar-biofilm-derived carbon and the activity of specific

sulfadiazine degraders (e.g., *Arthrobacter* D2; [24,26]), with only a minor contribution from mineralization (Fig. 1G), and (ii) physicochemical sequestration of extractable parent sulfadiazine in the high-BET-area biochar-biofilm composite (Supplementary, Table 6; Fig. 1D [27]), although the present mass-balance data do not quantify the relative contribution of these pathways. This dual mechanism effectively removes parent sulfadiazine from the bulk-soil compartment, shortening the effective exposure window and lowering concentration-dependent filtering. Consistent with this soil-dependent response, Ultisol differs from Mollisol in several mechanistically relevant properties (e.g., lower pH and SOM or DOC, lower CEC and nutrient availability, and a higher clay fraction; Supplementary Table 1), which can constrain intrinsic dissipation capacity while modulating sulfadiazine speciation and sorption or partitioning, thereby prolonging the exposure or selection window and increasing the marginal benefit of carrier-associated partitioning and biofilm microhabitats. The lower organic matter content and less abundant indigenous microbial community in the Ultisol compared with the Mollisol likely provided biofilm-associated sulfadiazine degraders (including *Arthrobacter* sp. strain D2) with more ecological space for growth and proliferation (Supplementary, Fig. 9), thereby potentially facilitating sulfadiazine biodegradation [28-30]. However, the specific quantitative contribution of the inoculated strain D2 relative to indigenous sulfadiazine degraders cannot be resolved from the current dataset.

In line with less efficient microbial degradation, final sulfadiazine concentrations within the biochar-biofilm composite were higher in the Ultisol than in the Mollisol. After the removal of the biochar-biofilm composite, the Ultisol retained less sulfadiazine than the Mollisol from which the biochar-biofilm composite had been removed. Taken together, these patterns suggest that the biochar-amended biofilm might act primarily as a sorptive sink [31], sequestering or partitioning extractable parent sulfadiazine into the biochar–biofilm matrix and thereby reducing its bulk-soil bioavailability, rather than consistently stimulating additional biodegradation in the bulk soil. Therefore, under the incubation timescale studied here, the dominant outcome is best viewed as short-term depletion of the extractable parent sulfadiazine pool through sequestration and/or transfer into unresolved unrecovered ^{13}C pools, potentially including non-extractable residues, rather than evidence for permanent destruction of sulfadiazine. Consequently, while our data robustly quantify this short-term depletion,

the molecular identity, stability, and potential remobilization of these unrecovered pools are likely condition-dependent and warrant longer-term aging, desorption, and product-resolved assessments. Accordingly, biochar-biofilm composite applications are likely to be most beneficial in soils with limited native degradative capacity. Based on these dissipation dynamics, a 14-day incubation was selected for subsequent DNA-SIP-based community analyses.

Formation of ^{13}C-DNA, bacterial community dynamics, and the role of strain D2

The more fertile Mollisol contained a significantly higher absolute abundance of 16S rRNA genes per gram of DNA than the less fertile Ultisol (Supplementary Fig. 3). Across treatments, 16S rRNA gene abundances were primarily detected at buoyant densities between 1.70 g mL^{-1} and 1.73 g mL^{-1} (Supplementary Fig. 4). Here, 'density' refers to the buoyant density of DNA in the CsCl gradient (g mL^{-1}); incorporation of ^{13}C into DNA increases buoyant density, allowing labeled heavy DNA to be separated from unlabeled light DNA [32]. The distribution of heavy DNA differed between the two soils. In the Ultisol, the densest fractions were strongly enriched, with maximum relative abundances ranging from 35.2% to 73.4% while in the Mollisol, the heavy DNA peak shifted toward lighter fractions, with the proportion of heavy DNA decreasing from 34.1–36.4% to 24.4–32.2% (Supplementary Table 10), i.e., the faster dissipation of sulfadiazine in the Mollisol did not correlate with larger uptake of the ^{13}C into bacterial biomass.

Procrustes analysis aligns the ordination of community composition with that of resistome composition; the low M^2 values and significant permutation tests indicate that shifts in bacterial taxa covary with shifts in ARG profiles, i.e., the resistome is more tightly coupled to the bacterial community than to archaea or eukaryotes in our SIP-resolved datasets. The results indicated that bacterial communities were the primary drivers of the antibiotic resistome (M^2 = 0.07), followed by eukaryotes and archaea (M^2 = 0.16 and 0.20, respectively; Fig. 2A). Among bacterial phyla, Actinobacteria showed the strongest concordance with the resistome (M^2 = 0.075; Supplementary, Table 11), with significant alignment in the Ultisol (p = 0.004) but not in the Mollisol (Fig. 2B). sulfadiazine concentrations were most strongly correlated with sulfonamide resistance genes. Among environmental variables, carbon-to-nitrogen ratios (C/N) showed a significant positive correlation with only three genera within the

Actinobacteria phylum (Supplementary Fig. 5A). These results indicate that, in the soils analyzed here, bacteria, rather than eukaryotes (e.g., fungi) or archaea, represent the primary carriers of sulfadiazine resistance determinants (Fig. 2). While fungi and archaea may participate in biotransformation or experience sulfadiazine-induced inhibition [33-35], viruses detected in the ^{13}C-DNA metagenomic datasets are most likely bacteriophages infecting sulfadiazine-degrading bacteria, rather than entities directly involved in sulfadiazine degradation processes [36].

Arthrobacter spp., including strain D2, were detected in the heavy-fraction DNA from all soil samples but at low relative abundances (ranging from 3.5×10^{-6} to 3.4×10^{-1}%) (Supplementary Fig. 7). *Arthrobacter* ranked 50th in relative abundance and was not significantly enriched among ^{13}C-sulfadiazine-degrading bacteria compared with other taxa (Fig. 5A). Notably, strain D2 became enriched following removal of the biochar-biofilm composite, accounting for 7.7 ± 1.8% of the biochar-biofilm bacterial community, whereas it remained close to the detection limit in the Ultisol (Fig. 5B, C). *Arthrobacter* species have been isolated from diverse habitats, such as wastewater, activated sludge, and soils, indicating strong adaptability and colonization potential in soil environments [37,38]. It is therefore plausible that *Arthrobacter* strain D2 migrated from the biochar carrier into the surrounding soil. However, in our experiment, the exogenous *Arthrobacter* strain D2 did not exert a lasting impact on the relative abundance of *Arthrobacter* in the soil, suggesting that native members of this genus remained dominant. Under low sulfadiazine concentrations, sulfadiazine-degrading *Arthrobacter* populations (including strain D2) likely relied on additional carbon sources other than sulfadiazine for growth, which is consistent with their broad metabolic versatility.

Divergent resistome responses and environmental risks

A clear separation between the community profiles of sulfadiazine degraders and sulfadiazine non-degraders was observed in the Ultisol but not in the Mollisol, which is consistent with differences in sulfadiazine persistence between soils. In the Ultisol, slower sulfadiazine dissipation likely extended the exposure window and imposed stronger selection, thereby promoting divergence between sulfadiazine degraders and sulfadiazine non-degrader assemblages, and promoting the above-mentioned uptake of sulfadiazine-derived ^{13}C-lable into bacterial DNA. In contrast, in the Mollisol,

faster sulfadiazine decline and higher overall microbial activity or competition likely reduced the duration and strength of selection, limiting detectable divergence.

This selective effect of sulfadiazine is consistent with previous studies showing that sulfadiazine addition alters bacterial community structure [39,40]. The higher relative abundance of *sul1* in non-degrading bacteria suggests a greater reliance on resistance mechanisms to persist under increased sulfadiazine stress, which exhibits bacteriostatic properties [41]. In addition to sulfadiazine, we detected measurable soil concentrations of ten other antibiotics (Supplementary, Fig. 8), which may have contributed to the higher prevalence of resistance observed in non-degrading communities. Moreover, Ultisols are generally characterized by lower availability of organic matter and nutrients than Mollisols, a condition that likely intensifies microbial competition and increases selective pressure for ARGs [42]. This constraint on microbial activity is supported by the significantly lower 16S rRNA gene copy numbers per gram of soil observed in the Ultisol compared to the Mollisol (Supplementary Fig. 3). Consequently, microbial communities in the Ultisol appear to be more adapted to sustained antibiotic loads but less capable of degrading sulfadiazine efficiently (Fig. 1C, E; Supplementary Fig. 1). In contrast, in the Mollisol, faster sulfadiazine decline combined with higher overall microbial activity and competitive interactions likely reduced the duration and strength of selection, thereby limiting detectable divergence at the community level.

Across all treatments, 54 ARGs and 13 MGEs were detected (Fig. 3A). PCoA indicated that soil type was the primary determinant of ARG composition (PCoA1 = 46.8%), while biochar-biofilm composite addition and sulfadiazine degraders status explained additional variation along the second axis (PCoA2 = 24.8%; Fig. 4A). These effects were supported by PERMANOVA based on Bray–Curtis dissimilarities (Supplementary, Table 12), including analyses with permutations restricted within soil strata as well as tests conducted separately within each soil. Because dispersion differences can influence ordination patterns, we additionally assessed homogeneity of multivariate dispersions (PERMDISP and betadisper; Supplementary Table 13). These robust ordination patterns suggest that selection on ARGs is closely linked to sulfadiazine-degrading dynamics at the community level under the combined effects of treatment and sulfadiazine degraders status, rather than being attributed to the presence and activity of a single inoculated taxon (e.g., *Arthrobacter* strain D2) based on ordination

alone. Importantly, resistome responses differed between SIP-resolved fractions. In Ultisol sulfadiazine degraders (^{13}C-DNA), biochar-biofilm composite amendment reduced both ARG richness and absolute abundance, whereas in the Mollisol the sulfadiazine-non-degrader fraction and the whole-community fraction ARG richness declined but the total absolute abundance (i.e., operational load) increased (Figs. 3B, C; Supplementary Table 14). Effect-size summaries based on the detected ARG table used in Fig. 4A showed that ARG_sum increased from 0.311 to 0.859 in Mollisol ^{12}C-DNA (Δ = +0.548; 95% CI: 0.317–0.840), whereas it decreased from 2.14 to 1.46 in Ultisol ^{13}C-DNA (Δ = −0.681; 95% CI: −0.805 to −0.557) (Supplementary, Table 14). Consistent with these patterns, in the Ultisol, the biochar-biofilm composite decreased multiple ARG classes, including aminoglycoside, chloramphenicol, MLSB, multidrug, sulfonamide, tetracycline, and trimethoprim, as well as three MGEs (transposase, insertion sequence, and integrase). In contrast, in the Mollisol, biochar-biofilm composite addition increased several ARG classes, including aminoglycoside, chloramphenicol, MLSB, multidrug, sulfonamide, and tetracycline, along with two MGEs (transposase and insertion sequence) (Fig. 3B and Supplementary Fig. 6). The main ARG features contributing to the Mollisol increase are summarized in Supplementary Table 14.

Crucially, these fraction-resolved results also clarify net risk interpretation: reductions observed within the SIP-defined sulfadiazine degraders fraction do not necessarily imply a net decrease of the whole-community resistome. In Mollisol, composite addition increased the operational whole-community (^{12}C-DNA) ARG load (Supplementary Table 14) and coincided with increases in multiple ARG classes and MGEs (Fig. 3B and Supplementary Fig. 6), suggesting a potential trade-off in more fertile soils, which aligns with recent evidence showing that nutrient enrichment (e.g., organic matter) can significantly elevate MGE and ARG abundances even without direct antibiotic selection [43]. Consistent with this pattern, the concentrations of the other ten background antibiotics in the more fertile Mollisol were all reduced on day 14 (Supplementary Fig. 8), potentially lowering selection for the corresponding ARGs in sulfadiazine-degrading bacteria by other antibiotics. Hence, high microbial activity alone could already potentially mitigate the ecological impact of antibiotic loads by enhancing degradation processes [44]; thereby rendering the additional mitigation by the biochar-biofilm composite largely redundant in this soil.

Targeted quantification of six sulfonamide resistance genes (*sul1*, *sul2*, *sul3*, *strB*, *sulA/folP*, and *folA*) showed that *sul2*, *sul3*, and *folA* were absent from sulfadiazine degraders communities in both soils [45]. Among the detected genes, *sul1* dominated the sulfonamide resistome, accounting for 4.8–28% of relative abundance (Fig. 4C). In the Ultisol, *sul1* was more abundant in sulfadiazine non-degraders than in sulfadiazine degraders and showed positive correlations with *tnpA_2* and *strB* (Fig. 4E). Within the Ultisol sulfadiazine-degrader fraction (^{13}C-DNA), amendment with the biochar-biofilm composite reduced *sul1* abundance by 22 ± 6.7% relative to the control (mean ± SD, n = 3 microcosms). In contrast, no reduction of *sul1* was observed in the Mollisol. Instead, biochar-biofilm composite addition increased the relative abundance of *strB* by 1.6- to 2.2-fold and *sulA/folP* by 4.6-fold in Mollisol degraders, whereas *sulA/folP* was not detected in the Ultisol (Fig. 4C). In preliminary experiments in which *Arthrobacter* strain D2 was incubated with sulfadiazine as the sole carbon source, *sulA/folP* was detected in strain D2, whereas *strB* was not (Fig. 4D). This observation suggests that *strB* did not originate from *Arthrobacter* strain D2 and that the addition of the biochar-biofilm composite may have promoted the growth or proliferation of other *strB*-hosting bacteria. Here, *sulA/folP* was detected in sulfadiazine-degrading bacteria in both biochar-biofilm composite treatments and control soils, indicating that *sulA/folP* was either already present in, or potentially transferred to, indigenous sulfadiazine-degrading bacteria. Similar patterns have been reported previously [46,47]. Thus, in the Mollisol, the biochar-biofilm composite appeared to amplify *sulA/fol*P in sulfadiazine-degrading bacteria rather than introducing these genes de novo.

Sulfadiazine-degrading Proteobacteria were strongly and positively correlated with plasmid replication gene abundance and carried high MGE loads (Supplementary, Fig. 5B), indicating that they are likely major hosts mediating plasmid-borne ARG transfer in soil. Because Proteobacteria are well known to transfer DNA across phyla via conjugation [48], their enrichment within the sulfadiazine-degrading fraction points to an elevated potential for horizontal ARG dissemination and, consequently, AMR. Consistent with this Proteobacteria-centered mechanism, the most enriched pathogenic genus among sulfadiazine degraders was *Bartonella*, a member of Proteobacteria, which has been reported to exchange genes with human intestinal bacteria [49]. Moreover, 16 pathogenic genera were more abundant in the sulfadiazine degraders than in the sulfadiazine non-degraders (Fig. 5F). Notably, these

risks were soil-type dependent: in the Mollisol, most sulfadiazine-degrading pathogens established poorly (accumulation factor < 0.5 for 90% of pathogenic taxa), likely reflecting stronger competitive exclusion by the native microbiota. Taken together, these results indicate that sulfadiazine-degrading communities dominated by Proteobacteria might increase opportunities for plasmid-borne ARG transfer, while soil-specific microbial interactions potentially modulate the establishment and persistence of potential pathogenic sulfadiazine degraders.

An exploratory correlation-based network analysis of ARGs, MGEs, and bacterial genera in sulfadiazine-degrading bacteria showed that key ARG and MGE nodes differed between Ultisol and Mollisol (Fig. 4E), suggesting soil-dependent co-occurrence patterns under sulfadiazine stress. Given the limited sample size used for network inference (n = 6 per soil), these associations should be interpreted as hypothesis-generating and do not by themselves demonstrate horizontal transfer or causal interactions. In Ultisol, a strong correlation was observed between *sul1* and *tnpA_2* ($\rho = 0.96$, n=6, $p = 0.034$), which is consistent with previous research [47,50]. Bacterial metabolism of sulfadiazine under high sulfadiazine concentrations might simultaneously promote the co-selection or co-mobilization of *sul1* and *tnpA_2*. A contig-based analysis revealed the composite ARG *sul1-tnpA*, while Antarctic soil-derived ARB exhibited simultaneously high abundances of *sul1* and *tnpA_2*, suggesting that *tnpA* might generally contribute to the horizontal transfer of *sul1* [47,51]. While a direct and significant correlation between *sul1* and *tnpA_2* was not observed in Mollisol, both exhibited strong associations with *ISSm2_Xanthob*, consistent with the potential co-occurrence of *sul1* with MGEs during sulfadiazine degradation. Under high sulfadiazine stress in both Ultisol and Mollisol, *sul1* was strongly correlated with some MGEs, suggesting that ARG–MGE co-occurrence may remain elevated while sulfadiazine persists, and motivating future validation with higher replication and/or contig-resolved evidence.

Mitigation of virulence factors and pathogenic bacteria

Following the addition of the biochar-biofilm composite, the total relative abundance of pathogenic bacteria and VFs decreased in both sulfadiazine-degrading and non-sulfadiazine-degrading communities (Fig. 5D, E). In the Ultisol, the most pronounced reductions were observed for VF

categories associated with stress response and iron uptake systems (Fig. 5E). In contrast, in the more fertile Mollisol, VF categories showed a more uniform decrease across most functional mechanisms. Regardless of biochar-biofilm composite addition, the total relative abundance of pathogenic bacteria remained lower in the Mollisol than in the Ultisol. As a biochar-biofilm composite carrier, biochar retains a substantial number of persistent surface free radicals, which can potentially disrupt the membranes of pathogenic bacteria [52]. The iron-rich composition of the Ultisol [53] could further promote the generation of such persistent surface free radicals [54,55]. These molecular features may have implications not only for ion adsorption but also for the expression of proteins associated with VFs [56], potentially modulating mechanisms related to stress proteins and the iron uptake system within VFs.

The accumulation factor for 16 pathogenic taxa in the Ultisol control soil was greater than 1, indicating preferential enrichment among sulfadiazine degraders relative to sulfadiazine non-degraders (Fig. 5F). Among these pathogenic bacteria, *Bartonella* showed particularly strong enrichment, with a 1.96-fold higher relative abundance among sulfadiazine degraders than among sulfadiazine non-degraders. However, the addition of the biochar-biofilm composite reduced the abundance of these pathogenic taxa. This reduction in VF abundance effectively mitigates the specific enrichment of pathogenic sulfadiazine degraders, particularly in the Ultisol.

Conclusions and environmental implications

To improve process-level resolution, future studies should integrate SIP with metatranscriptomics (or RT-qPCR targeting sulfadiazine-catabolic genes) and pathway-level functional profiling to better quantify the contribution of inoculated degraders and link resistome shifts to metabolic adaptation in situ. From an applied perspective, field-scale validation under manure-amended conditions is needed to test efficacy under heterogeneous and repeated-input scenarios and to determine whether the observed reduction in bioavailable sulfadiazine reflects durable remediation or primarily temporary sequestration. Such studies should also assess the long-term stability and potential remobilization of sequestered and unrecovered pools, as well as practical deployment strategies and cost-effective scale-up of the biochar-biofilm composite.

In conclusion, this study demonstrates that biochar-biofilm composite can enhance the depletion of

bulk-soil extractable parent sulfadiazine (i.e., operational 'removal' of the parent compound) in less fertile Ultisol, a soil type prevalent in subtropical and tropical agroecosystems. Given that cumulative $^{13}CO_2$ mineralization remained < 2% of the initial ^{13}C spike, and that the majority of the ^{13}C-sulfadiazine ended in the non-extractable pool, the fast dissipation of sulfadiazine and its 'removal' from the bioavailable fraction should be interpreted primarily as sequestration into the biochar composite, or microbially mediated bound-residue formation rather than to complete mineralization. Accordingly, the dominant benefit over the incubation timescale studied here is best viewed as short-term risk mitigation via reduced bioavailable exposure, while the long-term stability and potential remobilization of sequestered and unrecovered pools remain to be validated. These effects are most consistently explained by the redistribution of antibiotic residues, mitigation of microbial stress, and suppression of ARG proliferation within antibiotic-degrading communities. Notably, the reduced abundance of pathogenic bacteria observed in amended Ultisols suggests a potential dual benefit for soil health and food safety. In contrast, Mollisols, temperate grassland-derived soils characterized by higher organic matter content and microbial diversity, did not exhibit comparable responses. This difference likely reflects the greater intrinsic resilience of Mollisol microbial communities to antibiotic perturbations and is consistent with previous observations that biochar amendments often confer limited benefits in already fertile soils [57]. More broadly, these results suggest that under comparable manure-derived antibiotic inputs, biochar-biofilm composites are most effective in low-fertility or disturbed soils characterized by lower SOM or DOC and lower nutrient or CEC levels (Supplementary, Tables 1 and 2), where intrinsic antibiotic dissipation is limited, and exposure windows are longer.

Methods

Soil, manure, antibiotics, and biochar-biofilm composite

Soil samples were collected as composites from an Ultisol and Mollisol in Yingtan and Changchun, China, respectively (for soil properties, Supplementary, Table 1). Ultisols are known for their low fertility due to their inherently acidic nature and high phosphorus-fixing capacity, whereas Mollisols are among the most fertile soils globally, rich in organic matter and nutrients. Pig manure was obtained from a medium-intensive farm in Yingtan, China, after a 2-month composting process. The soil and

manure were air-dried, gently ground, and passed through a 0.85-mm sieve before use.

To simulate the dominant route by which veterinary antibiotics enter agricultural soils and to compare soil-type effects under a common exposure scenario, all soil samples were amended with 4% (w/w) pig manure collected from a local farm after two months of composting and were then homogenized by air-drying and sieving through a 0.85-mm mesh. The amended soils were pre-incubated at 25 ℃ for two weeks at 28% water-holding capacity to re-equilibrate the microbial communities. Moisture was replenished every two days during the pre-incubation. Subsequently, soils were amended with 20 mg kg^{-1} of $^{13}C_6$-sulfadiazine (99%; Cambridge Isotope Laboratories) and incubated for an additional 21 days. To quantify excess ^{13}C attributable to sulfadiazine degradation, a parallel set of non-labeled soils received unlabeled sulfadiazine at the same concentration. Sulfadiazine stock solutions were prepared in methanol and added to achieve the target concentration.

A portion of the soil samples was subjected to biofilm treatment using the Arthrobacter strain D2 grown on biochar carriers. The bacterial load was approximately 1.0×10^{11} colony-forming units g^{-1}. Bamboo biochar (0.6-0.85 mm) was used as the carrier material. prepared from bamboo biomass by oxygen-limited pyrolysis at 500 ℃, was used as the carrier material. For biochar preparation, bamboo biomass was washed with deionized water and oven-dried for 12 h, placed in lidded ceramic crucibles, heated to 500 °C at 10 °C min^{-1}, held for 2 h, and allowed to cool naturally in the closed furnace. The resulting biochar was gently ground and sieved to 0.60-0.85 mm for subsequent experiments. Scanning electron micrographs analyses confirmed that biofilms formed only on biochar, whereas no comparable structures were observed on montmorillonite, kaolin, or goethite (Supplementary Fig. 2), supporting the selection of biochar as the sole carrier. The physicochemical properties of the carrier, bamboo biochar, are documented in Supplementary Table 2. The biochar-biofilm composite was added in an amount of 40 g kg^{-1} soil.

Arthrobacter strain D2 was obtained from the laboratory of Professor Tong Zhang at The University of Hong Kong and cultivated in Luria-Bertani medium at 37 °C. After 24 h of incubation, cells were harvested, washed twice with sterile phosphate-buffered saline (PBS), resuspended in mineral salts medium, and adjusted to an optical density of 1 at 600 nm (OD_{600}). The mineral salts medium contained (per litre) 1.0 g $(NH_4)_2SO_4$, 0.2 g $MgSO_4\cdot7H_2O$, 0.1 g $CaCl_2$, 1.0 g K_2HPO_4, and 0.5 g KH_2PO_4; after sterilization and cooling to approximately 60 °C, 2 mL L^{-1} of Coleman Lab MSM metals solution was aseptically added. The metals solution contained (per litre) 6.37 g $Na_2EDTA\cdot2H_2O$, 1.0 g $ZnSO_4\cdot7H_2O$, 0.5 g $CaCl_2\cdot2H_2O$, 2.5 g $FeSO_4\cdot7H_2O$, 0.1 g $NaMoO_4\cdot2H_2O$, 0.1 g $CuSO_4\cdot5H_2O$, 0.2 g $CoCl_2\cdot6H_2O$,

0.52 g $MnSO_4 \cdot H_2O$, and 60.0 g $MgSO_4 \cdot 7H_2O$. The carrier biochar-based biofilm culture system was established by combining 8 mL of bacterial suspension (OD_{600} = 1), 32 mL of Luria-Bertani medium, and 4 g of biochar in a total volume of 40 mL. After natural sedimentation, the biochar-biofilm composite was washed twice with PBS and freeze-dried under vacuum at -80 °C. Biofilm biomass on biochar was calibrated by combining dry-weight measurements of lyophilized culture aliquots with colony-forming unit counts obtained by serial dilution plating.

Microcosm incubation, sampling, and chemical analyses

All treatments were conducted in triplicate. Soil and CO_2 gas samples were collected on days 0, 7, 14, and 21 of incubation using airtight incubation bottles equipped with gas-sampling ports. At each time point, headspace gas (20 mL) was withdrawn using a gas-tight syringe for CO_2 and $^{13}CO_2$ analysis, while soil subsamples were taken to determine ^{13}C-sulfadiazine concentrations. We then assessed the CO_2 concentration from soil respiration as well as the ^{13}C-sulfadiazine concentration in soil, together with the bulk $\delta^{13}C$ in soil, CO_2, and biochar-biofilm composite. In addition, DNA was extracted on day 14 before the remaining antibiotics were fully degraded (Supplementary, Fig. 1). Extractable parent ^{12}C- and ^{13}C-sulfadiazine were quantified separately for bulk soil and, where applicable, for the recovered biofilm fraction by liquid chromatography-triple quadrupole mass spectrometry (LCMS-8050, Shimadzu, Tokyo, Japan). The ^{13}C content of respired CO_2 was determined from headspace analyses using a gas chromatograph (Agilent 7890B, Agilent Technologies, Santa Clara, CA, USA) coupled to a MAT 253 isotope ratio mass spectrometer (Thermo Fisher Scientific, Bremen, Germany). Ambient air was periodically introduced into the bottles to maintain adequate oxygen levels.

In biofilm-amended microcosms, the recovered material was analyzed as a separate compartment (‘recovered biofilm fraction’). For the recovery procedure, freeze-dried soils were first gently disaggregated and passed through a 0.6-mm sieve to remove the fine soil fraction; biochar particles (0.60-0.85 mm) carrying attached biofilms were then manually sorted from the retained fraction. Loosely attached soil particles were removed using a soft brush to minimize soil carryover while avoiding damage to the biofilm matrix. The reported sulfadiazine concentrations for this fraction therefore represent extractable parent sulfadiazine recovered by solvent extraction and operationally reflect the extractable pool rather than total sorbed or intracellular sulfadiazine.

Extraction of ^{13}C-sulfadiazine from soil and the biochar-biofilm composite was performed using a modified QuEChERS method [24,58]. To assess background contamination, extracts were additionally screened for other antibiotics using liquid chromatography-triple quadrupole mass spectrometry

(LCMS-8050, Shimadzu, Tokyo, Japan), given that agricultural soils and manures may contain pre-existing antibiotic residues. In total, ten additional antibiotics were detected in the original soil. Analytical conditions and measured concentrations are provided in Supplementary Tables 4 and 5. Briefly, freeze-dried samples were ground to pass a 0.25-mm sieve and 1.5 g of homogenized material was amended with 2.0 mL Na_2EDTA solution (150 mg L^{-1}) in 50-mL polypropylene centrifuge tubes containing two ceramic homogenizers. After vortexing for 1 min, 5 mL acetonitrile:methanol (65:35, v/v) was added, followed by 2.0 g anhydrous Na_2SO_4 and 0.5 g NaCl. Samples were vortexed, centrifuged at 6000 g for 10 min, and 1.3 mL of supernatant was subjected to dispersive solid-phase extraction using C18 (12.5 mg), primary secondary amine (PSA; 12.5 mg), and Na_2SO_4 (225 mg). After mixing and centrifugation at 10000 g for 5 min, 1.0 mL of the supernatant was transferred to brown glass vials for LC-MS/MS analysis. The same extraction protocol was applied to biochar-biofilm composite and manure samples to assess background residues. Sulfadiazine spike-recovery tests were conducted in soil, manure, and biochar-biofilm matrices, and recoveries ranged from 76.0 ± 2.7% to 97.6 ± 0.4% across the tested matrices (Supplementary Table 3).

Visualization and composition analysis of biochar-biofilm composite

After fixing the biofilms with 2.5% glutaraldehyde, the microbes in the biofilm were added to the soil on day 0, and the biochar-biofilm composite recovered on day 14 was examined under a scanning electron microscope (HITACHI SU8010). In a carrier-screening experiment, scanning electron microscopy after 24 h showed bacterial attachment to montmorillonite and kaolin but no distinct biochar-biofilm composite structures, while little attachment was observed on goethite; in contrast, clear biofilms were observed on biochar. After 14 d of soil incubation, recovered biochar-biofilm composites still harboured different bacterial morphotypes and extracellular polymeric substances, supporting the use of biochar as the sole carrier material. Soil pH was measured in a 1:2.5 (w/v) soil:water suspension using a Mettler Toledo FE28-CN pH meter. Elemental C, H, N, and S were determined by dry combustion using an Elementar Vario EL Cube elemental analyser. The Brunauer-Emmett-and Teller surface areas of soils, biochar, and biochar-biofilm composite are summarized in Supplementary Table 6.

Microbiome Processing: Molecular and metagenomic analyses

DNA was extracted from soil using the FastDNA Spin Kit (MP Biomedicals, CA, USA), whereas DNA from Arthrobacter strain D2 was extracted using the OMEGA Bacterial DNA Kit D3350. Extracted DNA was quantified with a Qubit 3.0 fluorometer (Thermo Fisher Scientific, USA) and stored at -80 °C. ^{13}C-labeled DNA was isolated through cesium chloride (CsCl) ultracentrifugation (45,000 rpm, 45 h, 20 °C) [59]. The heavy DNA layer was identified based on 16S rRNA gene abundance, representing ^{13}C-enriched sulfadiazine degraders [60]. For buoyant-density fractionation, 16S rRNA gene copy numbers in individual gradients were quantified on a qTower 3G real-time PCR system (Analytik Jena, Germany) using TB Green Premix Ex Taq with primers 515F (5′-GTGCCAGCMGCCGCGG-3′) and 907R (5′-CCGTCAATTCMTTTRAGTTT-3′). Heavy and light DNA layers of each sample were subsequently pooled separately and stored at -80 °C. Additional qPCR conditions are summarized in Supplementary Tables 7 and 8.

High-throughput qPCR was conducted using the Takara SmartChip Real-time PCR system (100 nL per reaction) with automated dispensing via the Multisample Nanodispenser [45,61]. A total of 384 primer pairs were used to quantify ARGs, MGEs, and 16S rRNA genes in DNA from soil, manure, and Arthrobacter D2, including 96 primer pairs specific to heavy-layer DNA from labeled and non-labeled treatments (Supplementary Table 9). Genes detected in at least two of three replicates (Ct < 30) were considered valid [45,61,62]. Heavy-layer DNA from ^{12}C- and ^{13}C-sulfadiazine-treated soils was used for metagenomic sequencing (Illumina NovaSeq, Majorbio) to identify antibiotic-degrading microbes and virulence factors (VFs). For biochar-biofilm composite samples, full-length 16S rRNA gene sequencing (PacBio) was performed to resolve species-level taxonomy. Metagenomic libraries (~400 bp) were prepared using the NEXTFLEX Rapid DNA-Seq kit, and annotations were conducted against the NR and VFDB databases using DIAMOND and BLASTP ($e \leq 10^{-5}$).

Calculation of isotope metabolism and abundance of ARGs and microbes

The non-labeled treatments served as natural-abundance controls to calculate $\Delta\delta^{13}$C with Eq. (1), convert δ^{13}C to atom-% with Eq. (2), and partitioning of CO_2 into sulfadiazine-derived and soil-derived sources using a two-pool isotope-mixing model as Eq. (3). The relative abundance of ^{13}C in soil and CO_2 was expressed as the difference between the labeled and non-labeled treatments, yielding $\Delta\delta^{13}$C (‰) as follows: Eq. (1):

$$\Delta\delta^{13}\mathrm{C}\ (‰) = \delta^{13}\mathrm{C}_{labeled\ treatment} - \delta^{13}\mathrm{C}_{non-labeled\ treatment} \quad (1)$$

The $\delta^{13}C$ values were converted to atom-% using the VPDB standard ratio (R_standard = 0.0111802): $R_{sample}=R_{standard}(\frac{\delta^{13}C}{1000}+1)$.

$$\text{atom\%}^{13}C_{SDZ}=\frac{100\times R_{standard}\times\left(\frac{\delta^{13}C}{1000}+1\right)}{1+R_{standard}\times\left(\frac{\delta^{13}C}{1000}+1\right)} \quad (2)$$

The CO_2 efflux from ^{13}C-sulfadiazine soil was partitioned into ^{13}C-sulfadiazine-derived and soil-derived components with the two-pool isotope-mixing model Eq. (2) [45]. This model partitions the total CO_2 efflux from soil with ^{13}C-sulfadiazine into sulfadiazine-derived and soil-derived components based on ^{13}C atom-% mass balance.

$$CO_{2,\ \text{sulfadiazine}-derived}=CO_{2,total}\times\frac{\text{atom\%}\ \ ^{13}CO_{2,total}-\text{atom\%}\ \ ^{13}CO_{2,soil}}{\text{atom\%}\ \ ^{13}CO_{2,\text{sulfadiazine}}-\text{atom\%}\ \ ^{13}CO_{2,soil}} \quad (3)$$

Where CO_2, ^{13}C-sulfadiazine-derived, $CO_{2,\ soil}$, and $CO_{2,\ total}$ refer to the ^{13}C-sulfadiazine-derived CO_2-C, soil-derived CO_2-C, and total CO_2-C from soil with ^{13}C-sulfadiazine, respectively. Atom-% $^{13}CO_{2,\ \text{sulfadiazine-derived}}$, atom-% $^{13}CO_{2,\ soil}$, and atom-% $^{13}CO_{2\ total}$ are the ^{13}C atom-% values of the CO_2, derived from ^{13}C-sulfadiazine, non-labeled soil, and ^{13}C-sulfadiazine soil, respectively.

Calculation of mineralized ^{13}C-sulfadiazine in soil via $^{13}CO_2$ is shown in Supplementary Eq. (4).

$$\text{Mineralized}\ ^{13}C_6\text{-SDZ}=CO_{2\ \text{SDZ-derived}}\times\frac{6\times m_C\times m_{^{13}C_6\text{-SDZ}}}{m_{CO_2}} \quad (4)$$

In Eq.(5), $CO_{2,\ \text{SDZ-derived}}$ represents the mass of sulfadiazine-derived CO_2-C (mass of carbon), m_C is the molar mass of carbon, $m_{^{13}C_6}$-SDZ is the molar mass of fully $^{13}C_6$-labeled sulfadiazine, and "6" is the number of labeled carbons per molecule.

The relative gene copy number of ARG was calculated using Eq. (5) [62] with a cycle-threshold (Ct) detection limit of 30.

$$\text{Relative gene copy number} = 10^{\frac{30\text{-Ct}}{3.3333}} \quad (5)$$

The relative abundance of ARGs was then normalized to the 16S rRNA gene copy number using Eq. (6). following a previous report [63].

$$RA_{ARG}\ (\%) = \frac{\text{relative gene copy number}}{\text{relative gene copy number}_{16S\ rRNA\ gene}} \times 100 \quad (6)$$

For metagenomic datasets, the relative abundance of VFs and pathogenic taxa were normalized to the 16S rRNA gene copy number, Supplementary Eqs. (7, 8).

$$\text{normalized RA}_{\text{VFs}}\ (\%) = \frac{\text{read counts}_{(\text{VFs})}}{\text{relative gene copy number}_{(\text{16S rRNA gene})}} \times 100 \quad (7)$$

$$\text{normalized RA}_{\text{pathogenic bacteria}}\ (\%) = \frac{\text{reads number}_{(\text{pathogenic bacteria})}}{\text{relative gene copy number}_{(\text{16S rRNA gene})}} \times 100 \quad (8)$$

In Eqs. (7) and (8), read counts refer to quality-filtered mapped reads assigned to the VF catalogue or to the target pathogenic taxon, respectively, and relative gene copy number_16S denotes the sample-specific 16S rRNA gene copy number.

The accumulation factor was used to evaluate the enrichment of pathogenic bacteria in ^{13}C-labeled sulfadiazine degraders relative to sulfadiazine non-degraders, Eq. (9):

$$\text{accumulation factor} = \frac{\text{RA}(^{13}\text{C}_{\text{sulfadiazine}})}{\text{RA}(^{12}\text{C}_{\text{sulfadiazine}})} \quad (9)$$

Here, accumulation factor > 1 indicates a higher relative abundance of pathogenic bacteria in sulfadiazine-degrading bacteria (RA (^{13}C_sulfadiazine)) than in non-degrading ones (RA (^{12}C_sulfadiazine)), whereas an accumulation factor < 1 indicates the opposite.

For compartment-level ^{13}C mass balance, the initially applied ^{13}C-SDZ spike was partitioned into bulk-soil extractable parent SDZ (f_soil), recovered-biofilm-fraction extractable parent SDZ (f_biofilm), mineralized SDZ calculated from $^{13}CO_2$ production (f_mineralized; Eq. (4)), and an unrecovered ^{13}C pool calculated by difference:

$$\text{f\_unrecovered}\ (\%) = 100 - \text{f\_soil} - \text{f\_biofilm} - \text{f\_mineralized}. \quad (10)$$

The unrecovered pool represents ^{13}C in transformation products, bound residues, and/or biomass incorporation that was not quantified as extractable parent SDZ or mineralized $^{13}CO_2$

Data analysis

Initial data processing was performed in R (version 4.2.3). Because all microcosm treatments were conducted in triplicate (n = 3), we emphasize effect sizes (e.g., PERMANOVA R^2) and provide effect-size-based summaries with confidence intervals for key resistome metrics (Supplementary Table 14), while treating correlation-based network patterns as exploratory. One-way analysis of variance (ANOVA) was used to compare ARGs, community composition, and their relative abundances across treatments, and results were visualized as heatmaps using the packages ‘plyr’, ‘ggplot2’, and ‘stringr’. Histograms and line graphs were created in OriginPro 2023 (Learning Version). Multivariate differences in ARG (or community) profiles were assessed using Bray–Curtis dissimilarities and tested

by PERMANOVA (adonis2, vegan), including permutations restricted within soil strata where applicable (Supplementary Table 12). Homogeneity of multivariate dispersions was evaluated using PERMDISP/betadisper (Supplementary Table 13). Spearman's rank correlations among ARGs, MGEs, and bacterial genera were computed in R using the 'psych' package. Significant correlations ($\rho > 0.7$ and $p < 0.05$) were visualized through correlation networks in Gephi 0.10.1 and Cytoscape 3.9.1 to illustrate pairwise relationships [45].

Funding Statements

This work was supported by the Institute of Soil Science, Chinese Academy of Sciences (ISSAS2419), the National Natural Science Foundation of China (41977137, 42307048), the International Atomic Energy Agency Coordinated Research Project (D15022), the Center for Health Impacts of Agriculture (CHIA) of Michigan State University, and the Research Group Linkage Project from the Alexander von Humboldt Foundation. Zhi Mei acknowledges support from both the European Union's Horizon Europe research and innovation programme under the Marie Skłodowska-Curie grant agreement No. 101206348 and the DAAD-Stiftung (trustee: DAAD e.V.), funded through private donations from Hauser & Friends. Jose Luis. Balcazar acknowledges support from the CERCA Programme of the Catalan Government.

Data availability

The source data underlying the main-text and supplementary figures of this study, including Supplementary Table 9 in editable format, are publicly available in Zenodo (DOI: 10.5281/zenodo.19612632) [66]. The raw metagenomic sequencing data and 16S rRNA gene amplicon data supporting the findings of this study have been deposited in the NCBI BioProject database under accession numbers PRJNA1055873 and PRJNA1062695, respectively.

Code availability

The code used for data processing, statistical analyses, and figure generation is publicly available in Zenodo (DOI: 10.5281/zenodo.19609305) [67].

Author information

Authors and Affiliations

State Key Laboratory of Soil & Sustainable Agriculture, Institute of Soil Science, Chinese Academy of Sciences, Nanjing, China

Zhi Mei, Fang Wang, Chao He, Maoyuan Liao, Yuhao Fu, Xin Jiang & Zhongjun Jia

Catalan Institute for Water Research (ICRA-CERCA), Girona, Spain

Zhi Mei & Jose Luis Balcazar

University of Chinese Academy of Sciences, Beijing, China

Zhi Mei, Fang Wang, Maoyuan Liao, Yuhao Fu & Xin Jiang

Institute of Crop Science and Resource Conservation (INRES) – Soil Science and Soil Ecology, University of Bonn, Bonn, Germany

Zhi Mei & Wulf Amelung

Joint FAO/IAEA Centre of Nuclear Techniques in Food and Agriculture, International Atomic Energy Agency, Vienna, Austria

Fang Wang

Institute of Comprehensive Utilization of Resources, Kunming Metallurgical Research Institute Co., Ltd., Kunming, China

Chao He

Department of Chemistry, Hong Kong Baptist University, Kowloon Tong, Hong Kong, China

Kelvin Sze-Yin Leung

Department of Civil and Environmental Engineering, Michigan State University, East Lansing, MI, USA

Syed A. Hashsham & James M. Tiedje

State Key Laboratory of Black Soils Conservation and Utilization, Northeast Institute of Geography and Agroecology, Chinese Academy of Sciences, Changchun, China

Zhongjun Jia

Environmental Microbiome Engineering and Biotechnology Laboratory, Department of Civil Engineering, The University of Hong Kong, Hong Kong, China

Tong Zhang

Agrosphere Institute (IBG-3), Forschungszentrum Jülich GmbH, Jülich, Germany

Wulf Amelung

Contributions

Zhi Mei conceived the study together with Fang Wang and designed the experiments. Zhi Mei performed all experiments, carried out all data analyses, prepared the original draft, and revised the manuscript throughout the review process. Fang Wang supervised the study, contributed to experimental design, and revised the manuscript. Wulf Amelung advised on data analysis and manuscript writing. Chao He did part of the data analysis and manuscript revision. Maoyuan Liao assisted with part of the experiments. Xin Jiang and Zhongjun Jia provided technical support and laboratory resources for key experiments. Tong Zhang provided the Arthrobacter strain and relevant strain information. Jose Luis Balcazar, Kelvin Sze-Yin Leung, Yuhao Fu, Syed A. Hashsham, Zhongjun Jia, Tong Zhang, and James M. Tiedje provided constructive comments on the manuscript. Fang Wang, Xin Jiang, and Zhi Mei funded the study.

Corresponding author

Correspondence to Fang Wang

Ethics approval and consent to participate

Not applicable. This study did not involve human participants, human data, or animal experiments.

Competing interests

The authors declare no competing interests.

Reference:

1. Van Boeckel, T. P. et al. Reducing antimicrobial use in food animals. *Science* **357**, 1350–1352 (2017).
2. Oliver, J. P. et al. Invited review: Fate of antibiotic residues, antibiotic-resistant bacteria, and antibiotic resistance genes in US dairy manure management systems. *J. Dairy Sci.* **103**, 1051–1071 (2020).
3. He, Y. et al. Antibiotic resistance genes from livestock waste: occurrence, dissemination, and treatment. *npj Clean Water* **3**, 4 (2020).
4. Cycoń, M., Mrozik, A. & Piotrowska-Seget, Z. Antibiotics in the soil environment—degradation and their impact on microbial activity and diversity. *Front. Microbiol.* **10**, 338 (2019).
5. Andersson, D. I. & Hughes, D. Microbiological effects of sublethal levels of antibiotics. *Nat. Rev. Microbiol.* **12**, 465–478 (2014).
6. United Nations Environment Programme. *Bracing for superbugs: strengthening environmental action in the One Health response to antimicrobial resistance*. https://www.unep.org/resources/superbugs/environmental-action (2023).
7. Wang, F. et al. Emerging contaminants: A One Health perspective. *Innovation* **5**, 100612 (2024).
8. Gatica, J. et al. Resistance of undisturbed soil microbiomes to ceftriaxone indicates extended spectrum β-lactamase activity. *Front. Microbiol.* **6**, 1233 (2015).
9. Rosendahl, I. et al. Persistence of the fluoroquinolone antibiotic difloxacin in soil and lacking effects on nitrogen turnover. *J. Environ. Qual.* **41**, 1275–1283 (2012).
10. Kopmann, C. et al. Abundance and transferability of antibiotic resistance as related to the fate of sulfadiazine in maize rhizosphere and bulk soil. *FEMS Microbiol. Ecol.* **83**, 125–134 (2013).
11. Jechalke, S. et al. Increased abundance and transferability of resistance genes after field application of manure from sulfadiazine-treated pigs. *Appl. Environ. Microbiol.* **79**, 1704–1711 (2013).
12. Jechalke, S., Heuer, H., Siemens, J., Amelung, W. & Smalla, K. Fate and effects of veterinary antibiotics in soil. *Trends Microbiol.* **22**, 536–545 (2014).
13. Wang, L. et al. Distribution characteristics of antibiotic resistant bacteria and genes in fresh and composted manures of livestock farms. *Sci. Total Environ.* **695**, 133781

(2019).

14. Rosendahl, I. et al. Dissipation and sequestration of the veterinary antibiotic sulfadiazine and its metabolites under field conditions. *Environ. Sci. Technol.* **45**, 5216–5222 (2011).
15. Förster, M. et al. Sequestration of manure-applied sulfadiazine residues in soils. *Environ. Sci. Technol.* **43**, 1824–1830 (2009).
16. Ostermann, A. et al. Leaching of veterinary antibiotics in calcareous Chinese croplands. *Chemosphere* **91**, 928–934 (2013).
17. Huang, X., Wen, D. & Wang, J. Radiation-induced degradation of sulfonamide and quinolone antibiotics: A brief review. *Radiat. Phys. Chem.* **215**, 111373 (2024).
18. Zhang, Q.-Q., Ying, G.-G., Pan, C.-G., Liu, Y.-S. & Zhao, J.-L. Comprehensive evaluation of antibiotics emission and fate in the river basins of China: source analysis, multimedia modeling, and linkage to bacterial resistance. *Environ. Sci. Technol.* **49**, 6772–6782 (2015).
19. Li, H. Z. et al. Active antibiotic resistome in soils unraveled by single-cell isotope probing and targeted metagenomics. *Proc. Natl Acad. Sci. USA* **119**, e2201473119 (2022).
20. Chen, J., Chen, X., Zhu, Y., Yan, S. & Xie, S. New insights into bioaugmented removal of sulfamethoxazole in sediment microcosms: degradation efficiency, ecological risk and microbial mechanisms. *Microbiome* **12**, 43 (2024).
21. Xiang, L. et al. Integrating biochar, bacteria, and plants for sustainable remediation of soils contaminated with organic pollutants. *Environ. Sci. Technol.* **56**, 16546–16566 (2022).
22. Dong, Q., LeFevre, G. H. & Mattes, T. E. Black carbon impacts on *Paraburkholderia xenovorans* strain LB400 cell enrichment and activity: implications toward lower-chlorinated polychlorinated biphenyls biodegradation potential. *Environ. Sci. Technol.* **58**, 3895–3907 (2024).
23. Engelhardt, I. et al. Fate of the antibiotic sulfadiazine in natural soils: experimental and numerical investigations. *J. Contam. Hydrol.* **177–178**, 30–42 (2015).
24. Mei, Z. et al. Biofilm enhanced the mitigations of antibiotics and resistome in sulfadiazine and trimethoprim co-contaminated soils. *J. Hazard. Mater.* **479**, 135721 (2024).

25. Zarfl, C., Klasmeier, J. & Matthies, M. A conceptual model describing the fate of sulfadiazine and its metabolites observed in manure-amended soils. *Chemosphere* **77**, 720–726 (2009).

26. Deng, Y., Mao, Y. P., Li, B., Yang, C. & Zhang, T. Aerobic degradation of sulfadiazine by *Arthrobacter* spp.: kinetics, pathways, and genomic characterization. *Environ. Sci. Technol.* **50**, 9566–9575 (2016).

27. Fu, Y. et al. Combating antibiotic resistance in the human-impacted environment with carbon-based materials: applications and challenges. *Crit. Rev. Environ. Sci. Technol.* **54**, 699–721 (2024).

28. He, Y., Yang, M., Huang, R., Wang, Y. & Ali, W. Soil organic matter and clay zeta potential influence aggregation of a clayey red soil (Ultisol) under long-term fertilization. *Sci. Rep.* **11**, 20498 (2021).

29. Huang, S., Peng, X. X., Huang, Q. R. & Zhang, W. J. Soil aggregation and organic carbon fractions affected by long-term fertilization in a red soil of subtropical China. *Geoderma* **154**, 364–369 (2010).

30. Liu, X. et al. Organic amendment improves rhizosphere environment and shapes soil bacterial community in black and red soil under lead stress. *J. Hazard. Mater.* **416**, 125805 (2021).

31. Kookana, R. S. The role of biochar in modifying the environmental fate, bioavailability, and efficacy of pesticides in soils: A review. *Aust. J. Soil Res.* **48**, 627–637 (2010).

32. Mei, Z. et al. Antibiotic-degrading bacteria shape resistome dynamics and horizontal gene transfer potential in soils with contrasting properties. *ISME Commun.* **6**, ycaf246 (2026).

33. Arun, K. B. et al. Filamentous fungi for pharmaceutical compounds degradation in the environment: A sustainable approach. *Environ. Technol. Innov.* **31**, 103182 (2023).

34. Zhao, S. et al. Sulfadiazine degradation by *Bjerkandera adusta* DH0817 at low temperatures and its cold-adaptation mechanisms. *Bioresour. Technol.* **407**, 131108 (2024).

35. Liao, Q. et al. Impacts of Cu and sulfadiazine on soil potential nitrification and diversity of ammonia-oxidizing archaea and bacteria. *Environ. Pollut. Bioavail.* **31**, 60–69 (2019).

36. Burmeister, A. R. et al. Pleiotropy complicates a trade-off between phage resistance and antibiotic resistance. *Proc. Natl Acad. Sci. USA* **117**, 11207–11216 (2020).

37. McCann, C. M. et al. Understanding drivers of antibiotic resistance genes in high Arctic soil ecosystems. *Environ. Int.* **125**, 497–504 (2019).

38. Busse, H.-J. & Wieser, M. in *The Prokaryotes: Actinobacteria* (eds Rosenberg, E. et al.) 105–132 (Springer, 2014).

39. Hammesfahr, U., Heuer, H., Manzke, B., Smalla, K. & Thiele-Bruhn, S. Impact of the antibiotic sulfadiazine and pig manure on the microbial community structure in agricultural soils. *Soil Biol. Biochem.* **40**, 1583–1591 (2008).

40. Zielezny, Y., Groeneweg, J., Vereecken, H. & Tappe, W. Impact of sulfadiazine and chlorotetracycline on soil bacterial community structure and respiratory activity. *Soil Biol. Biochem.* **38**, 2372–2380 (2006).

41. Venkatesan, M. et al. Molecular mechanism of plasmid-borne resistance to sulfonamide antibiotics. *Nat. Commun.* **14**, 4031 (2023).

42. Chen, Q.-L. et al. Cross-biome antibiotic resistance decays after millions of years of soil development. *ISME J.* **16**, 1864–1867 (2022).

43. Fu, Y. et al. Field-based evidence for the prevalence of soil antibiotic resistomes under long-term antibiotic-free fertilization. *Environ. Int.* **195**, 109202 (2025).

44. Ni, Z., Zhang, X., Guo, S., Pan, H. & Gong, Z. Impact of temperature elevation on microbial communities and antibiotic degradation in cold region soils of northeast China. *Toxics* **12**, 667 (2024).

45. Wang, F. et al. Long-term effect of different fertilization and cropping systems on the soil antibiotic resistome. *Environ. Sci. Technol.* **52**, 13037–13046 (2018).

46. Ji, X. et al. Antibiotic resistance gene abundances associated with antibiotics and heavy metals in animal manures and agricultural soils adjacent to feedlots in Shanghai, China. *J. Hazard. Mater.* **235–236**, 178–185 (2012).

47. Zhang, J. et al. Metagenomics insights into the profiles of antibiotic resistome in combined sewage overflows from reads to metagenome assembly genomes. *J. Hazard. Mater.* **429**, 128277 (2022).

48. Jiang, X. et al. Dissemination of antibiotic resistance genes from antibiotic producers to pathogens. *Nat. Commun.* **8**, 15784 (2017).

49. Schröder, G., Schülein, R., Quebatte, M. & Dehio, C. Conjugative DNA transfer

into human cells by the *VirB/VirD4* type IV secretion system of the bacterial pathogen *Bartonella henselae*. *Proc. Natl Acad. Sci. USA* **108**, 14643–14648 (2011).

50. Xu, C., Lu, J., Shen, C., Wang, J. & Li, F. Deciphering the mechanisms shaping the plastisphere antibiotic resistome on riverine microplastics. *Water Res.* **225**, 119192 (2022).
51. Na, G. S. et al. Occurrence and antibacterial resistance of culturable antibiotic-resistant bacteria in the Fildes Peninsula, Antarctica. *Mar. Pollut. Bull.* **162**, 111829 (2021).
52. Liao, S., Pan, B., Li, H., Zhang, D. & Xing, B. Detecting free radicals in biochars and determining their ability to inhibit the germination and growth of corn, wheat and rice seedlings. *Environ. Sci. Technol.* **48**, 8581–8587 (2014).
53. Yu, H. Y. et al. in *Advances in Agronomy* Vol. **137** (ed. Sparks, D. L.) 279–317 (Academic Press, 2016).
54. Fang, G., Liu, C., Gao, J., Dionysiou, D. D. & Zhou, D. Manipulation of persistent free radicals in biochar to activate persulfate for contaminant degradation. *Environ. Sci. Technol.* **49**, 5645–5653 (2015).
55. Zhang, P., Duan, W., Peng, H., Pan, B. & Xing, B. Functional biochar and its balanced design. *ACS Environ. Au* **2**, 115–127 (2022).
56. Xiao, X., Chen, B., Chen, Z., Zhu, L. & Schnoor, J. L. Insight into multiple and multilevel structures of biochars and their potential environmental applications: A critical review. *Environ. Sci. Technol.* **52**, 5027–5047 (2018).
57. Borchard, N., Siemens, J., Ladd, B., Möller, A. & Amelung, W. Application of biochars to sandy and silty soil failed to increase maize yield under common agricultural practice. *Soil Tillage Res.* **144**, 184–194 (2014).
58. Chuang, Y.-H., Zhang, Y., Zhang, W., Boyd, S. A. & Li, H. Comparison of accelerated solvent extraction and quick, easy, cheap, effective, rugged and safe method for extraction and determination of pharmaceuticals in vegetables. *J. Chromatogr. A* **1404**, 1–9 (2015).
59. Wei, W. et al. *Parabacteroides distasonis* uses dietary inulin to suppress NASH via its metabolite pentadecanoic acid. *Nat. Microbiol.* **8**, 1534–1548 (2023).
60. Cleary, D. M. et al. Capillary absorption spectroscopy for high temporal resolution measurements of stable carbon isotopes in soil and plant-based systems. *Plant*

Physiol. Biochem. **169**, 1–8 (2021).

61. Wang, F. et al. Influence of soil characteristics and proximity to Antarctic research stations on abundance of antibiotic resistance genes in soils. *Environ. Sci. Technol.* **50**, 12621–12629 (2016).
62. Looft, T. et al. In-feed antibiotic effects on the swine intestinal microbiome. *Proc. Natl Acad. Sci. USA* **109**, 1691–1696 (2012).
63. Mei, Z. et al. Bioaccumulation of manure-borne antibiotic resistance genes in carrot and its exposure assessment. *Environ. Int.* **157**, 106830 (2021).
64. Soil Survey Staff. *Keys to Soil Taxonomy* 8th edn (United States Department of Agriculture, 1998).
65. Xu, M. et al. Composting increased persistence of manure-borne antibiotic resistance genes in soils with different fertilization history. *Sci. Total Environ.* **689**, 1172–1180 (2019).
66. Mei, Z. & Wang, F. Source data for: Biochar-based composite drives sulfadiazine sequestration and mitigates active resistome risks. Zenodo https://doi.org/10.5281/zenodo.19612633 version 2 (2026).
67. Mei, Z. & Wang, F. Code for: Biochar-based composite drives sulfadiazine sequestration and mitigates active resistome risks. Zenodo https://doi.org/10.5281/zenodo.19609305 (2026).

Figure Captions

Fig. 1 | Distribution and transformation of ^{13}C-sulfadiazine in Ultisol and Mollisol with or without biochar–biofilm amendment.

A, Degradation of sulfadiazine (SDZ) in the soils at different incubation times. B, First-order kinetics fitting for sulfadiazine degradation in different treated soils. C, Percentage distribution of extractable parent SDZ between bulk soil and the recovered biofilm fraction (biochar carrier plus attached biofilm, separated from soil) at day 14 and day 21. D, Compartment-level ^{13}C mass balance of the initially applied ^{13}C-SDZ into bulk-soil extractable parent SDZ, biochar–biofilm composite extractable parent SDZ, mineralized $^{13}CO_2$, and unrecovered ^{13}C (by difference) at day 14 and day 21. Unrecovered ^{13}C represents transformation products, bound residues, and biomass incorporation. E, Concentration (mg kg^{-1}) of extractable parent SDZ in bulk soil and in the recovered biofilm fraction at day 14 and day 21. F, δ^{13}C of CO_2 derived from soil respiration over time. G, Cumulative proportion (%) of mineralized ^{13}C-SDZ over different incubation periods. Error bars in E–G represent s.d. Ul, Ultisol; Mo, Mollisol; Control, soil without biochar–biofilm composite; biofilm, soil amended with biochar–biofilm composite; ^{12}C, soil treated with unlabeled SDZ; ^{13}C, soil treated with ^{13}C-labeled SDZ; Ul_bio and Mo_bio denote the recovered biofilm fractions from Ultisol and Mollisol, respectively. Different lowercase letters indicate significant differences among treatments within the same sampling time (one-way ANOVA, $p < 0.05$).

Fig. 2 | Coupling of sulfadiazine-degrading communities with the antibiotic resistome across domains and soil types.

A, Consistency analysis for the sulfadiazine-degrading microbial community (bacteria, archaea, eukaryotes, and viruses) and the antibiotic resistome based on non-metric multidimensional scaling (NMDS) of species and antimicrobial resistance genes relative abundance. B, Consistency analysis of sulfadiazine-degrading bacteria and the antibiotic resistome in Ultisol and Mollisol. In each subplot, coloured circles and matching coloured triangles denote paired sample positions in the two ordinations, and blue arrows connect matched points. M^2 denotes the Procrustes sum of squares; P values were obtained by permutation tests (999 permutations).

Fig. 3 | Antimicrobial resistance genes and mobile genetic elements in sulfadiazine-degrading bacteria.

A, Relative abundance (RA) of all detected ARGs and mobile genetic elements (MGEs). B/C, Absolute abundance/detected number of ARGs with different resistance classes in the heavy layer DNA of different treated soils. In A, heatmap colours change from white to dark red with increasing RA, and grey cells indicate no detection. In B and C, blue bars denote control soils and magenta bars denote biofilm-amended soils within each soil-specific subplot; inset panels show enlarged views of low-abundance classes. Error bars represent s.d. ^{13}C indicates heavy-layer DNA from soil treated with ^{13}C-labeled sulfadiazine, corresponding to sulfadiazine-degrading bacteria. ^{12}C indicates heavy-layer DNA from the ^{12}C-sulfadiazine treatment, corresponding to non-sulfadiazine-degrading bacteria. Asterisks indicate significant differences between treatments ($p < 0.05$).

Fig. 4 | Resistome structure, sulfonamide resistance genes and ARG–host association networks in heavy-layer DNA and the D2 enrichment culture.

A, Principal coordinate analysis (PCoA) of ARG profiles (all detected ARGs) in the heavy layers of ^{12}C-sulfadiazine and ^{13}C-sulfadiazine treated soils, based on Bray–Curtis dissimilarities of relative abundance. PERMANOVA (adonis2) results for ARG profiles are provided in Supplementary Table 12; homogeneity of multivariate dispersions (PERMDISP and betadisper) is provided in Supplementary Table 13. B, PCoA of microbial community composition in the same heavy-layer DNA samples, based on Bray–Curtis dissimilarities of relative abundances. C, Relative abundance of sulfonamide resistance genes. Genes *sul2, sul3*, and *folA* were not detected in any sample and are not shown here. Asterisks indicate significant differences ($p < 0.05$). D, Relative abundance of sulfonamide resistance genes and MGEs detected in D2 bacteria under incubation conditions with sulfadiazine as the sole carbon source. Heatmap colours change from white to dark red with increasing relative abundance, and grey cells indicate no detection. E, Network analysis comparing the co-occurrence patterns of ARGs. A connection represents a strong (Spearman's correlation coefficient $\rho > 0.7$) correlation between the ARG subtype and MGE subtype and bacterial genera; coefficient $\rho > 0.7$) and significant ($p < 0.05$, $n > 5$) correlation. Only bacteria associated with ARGs or MGEs are shown, with no correlations within different bacteria.

Fig. 5 | Enrichment of *Arthrobacter* strain D2 and shifts in pathogenic bacteria and virulence factors.

A, Relative abundance of the top 50 bacterial genera. *Arthrobacter* is the 50th most abundant bacterial genera. B, Relative abundance of *Arthrobacter* strain D2 in the bulk soil compartment for Ultisol and Mollisol microcosms under control and biofilm-amended treatments (samples collected at day 14), based on metagenomic sequencing of species information. C, Relative abundance of *Arthrobacter* strain D2 in the recovered biochar–biofilm composite, from the biofilm-amended treatments at day 14 based on 16S rRNA gene full-length sequencing species information. ND indicates below the detection limit. Error bars represent s.d. D, Relative abundance of pathogenic bacteria in soil that received different treatments. E, Relative abundance of virulence factors (VFs) is categorized based on mechanisms levels. Level 1 is shown in different patterns in the Figure, and level 2 is shown in different colors in the Figure. F, Accumulation factors (AFs) of pathogenic bacteria of sulfadiazine-degrading bacteria in soils.

Editorial summary:

Biochar-biofilm carrying >i<Arthrobacter>/i< D2 reduced antimicrobial resistance genes and virulence factors in less fertile Ultisol, whereas more fertile Mollisol showed community resilience, based on DNA-stable isotope probing of soil samples.

Peer review information:

Communications Earth and Environment thanks Meredith Barr, Kunzheng Cai and Anlei Wei for their contribution to the peer review of this work.
Primary Handling Editors: Leiyi Chen and Somaparna Ghosh
A peer review file is available.

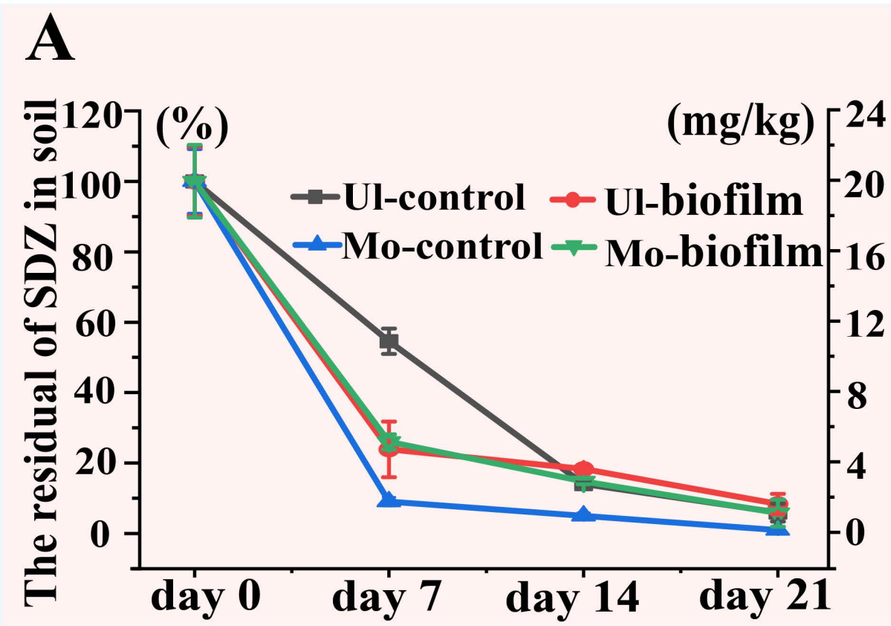
A
The residual of SDZ in soil
(%)
(mg/kg)
Ul-control
Ul-biofilm
Mo-control
Mo-biofilm
day 0
day 7
day 14
day 21

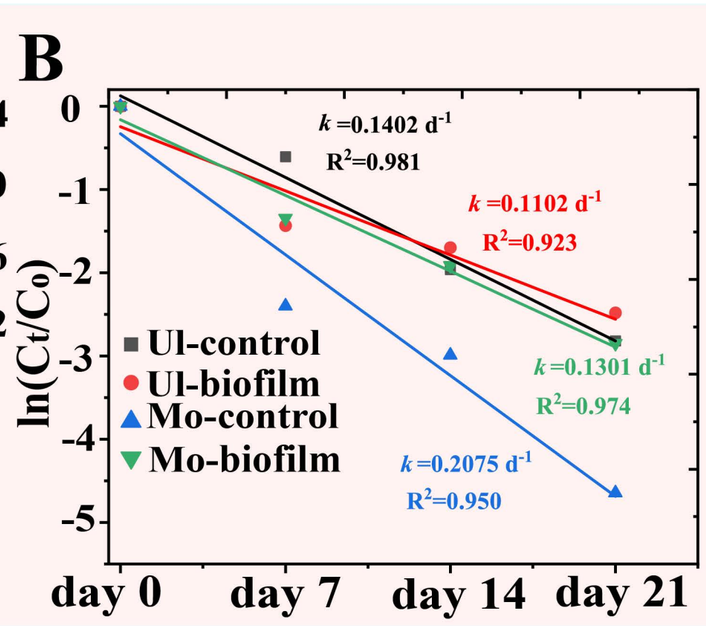
B
ln(Ct/C0)
k =0.1402 d-1
R2=0.981
k =0.1102 d-1
R2=0.923
k =0.1301 d-1
R2=0.974
k =0.2075 d-1
R2=0.950
Ul-control
Ul-biofilm
Mo-control
Mo-biofilm
day 0
day 7
day 14
day 21

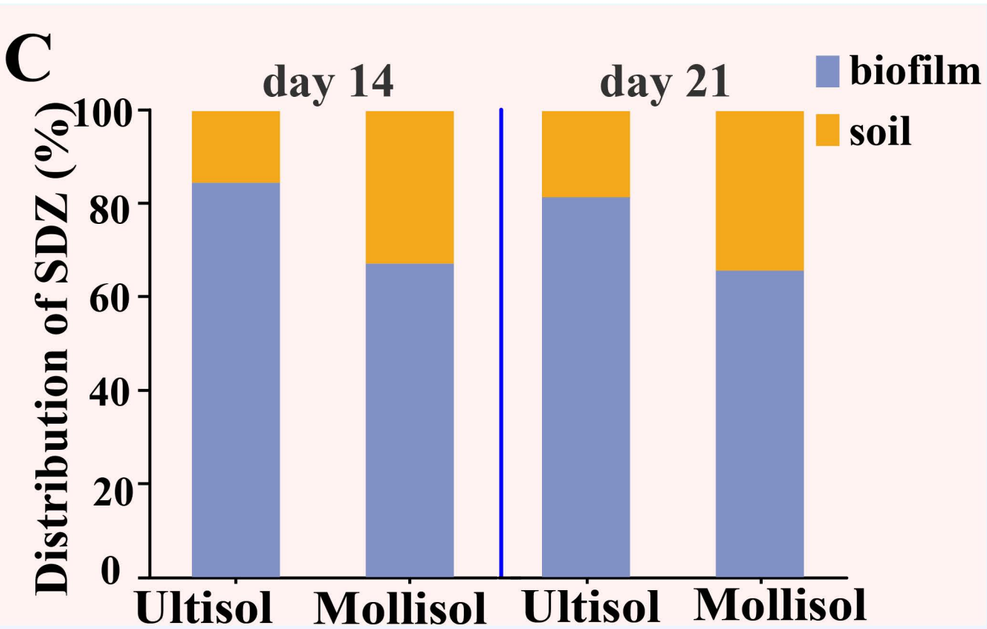
C
Distribution of SDZ (%)
day 14
day 21
biofilm
soil
Ultisol
Mollisol
Ultisol
Mollisol

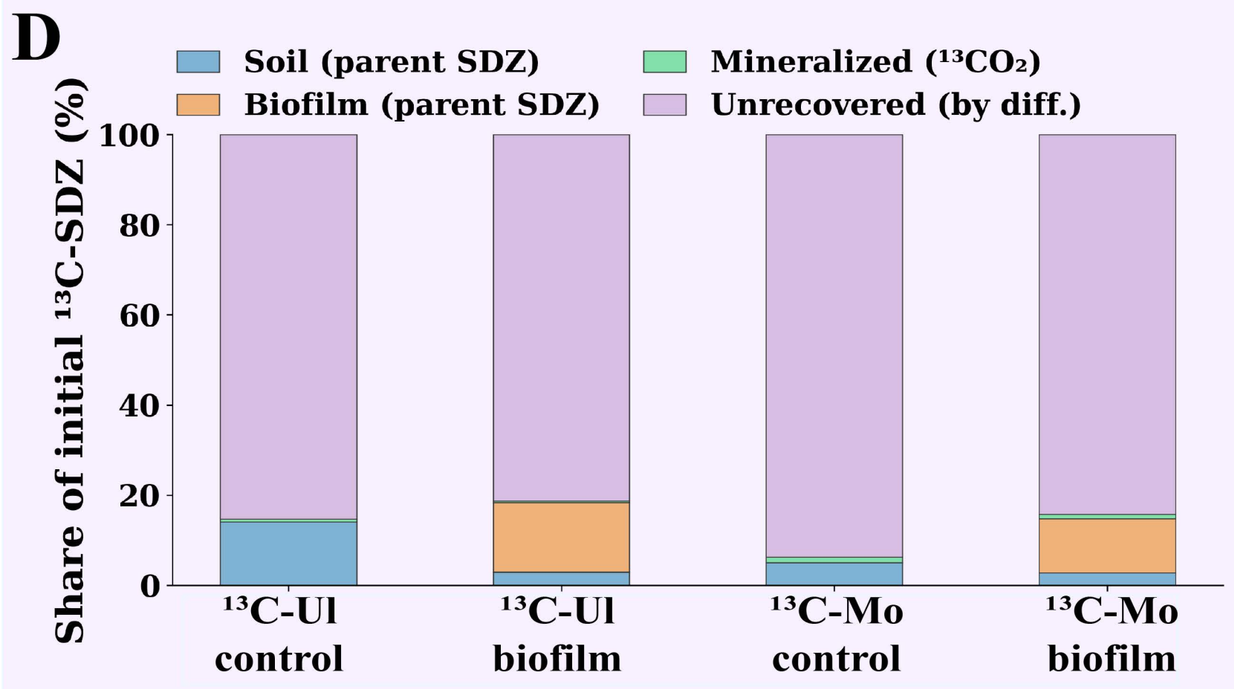
D
Soil (parent SDZ)
Biofilm (parent SDZ)
Mineralized (13CO2)
Unrecovered (by diff.)
Share of initial 13C-SDZ (%)
13C-Ul control
13C-Ul biofilm
13C-Mo control
13C-Mo biofilm
Day 14

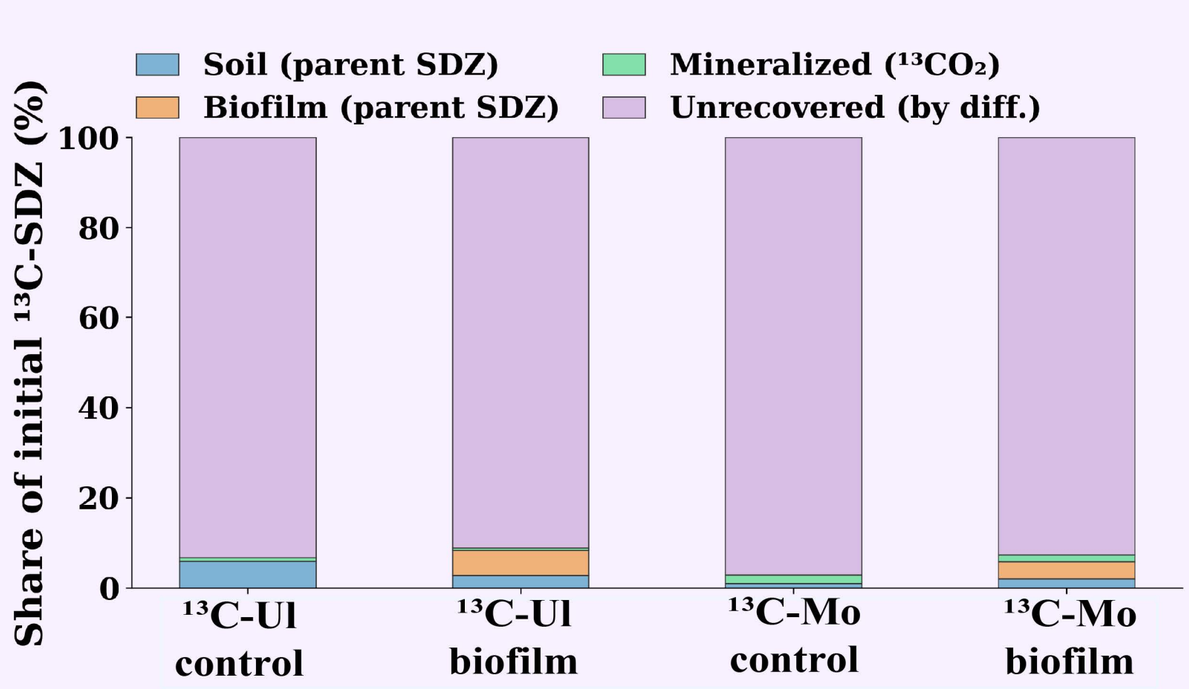
Soil (parent SDZ)
Biofilm (parent SDZ)
Mineralized (13CO2)
Unrecovered (by diff.)
Share of initial 13C-SDZ (%)
13C-Ul control
13C-Ul biofilm
13C-Mo control
13C-Mo biofilm
Day 21

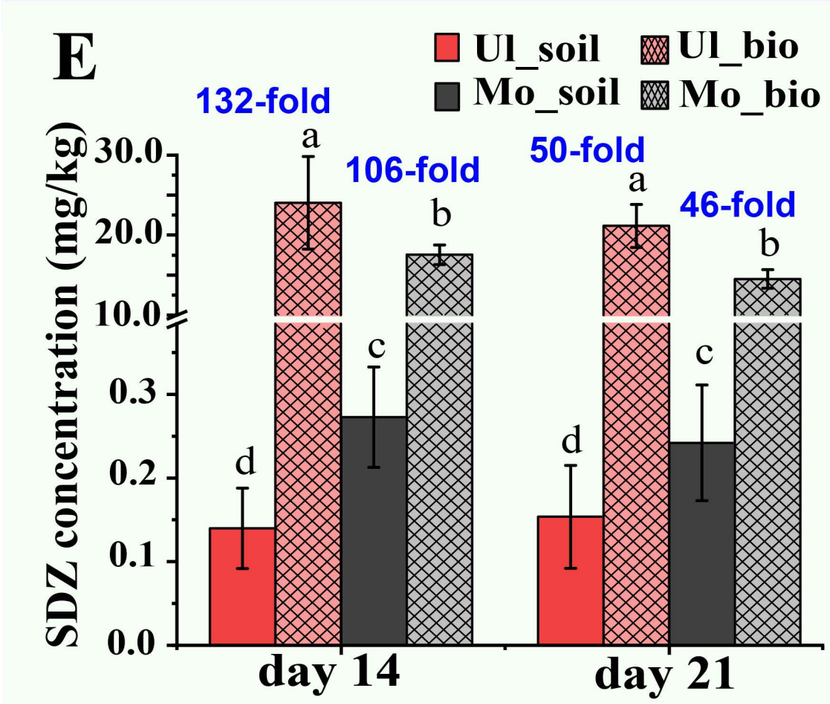
E
Ul_soil
Ul_bio
Mo_soil
Mo_bio
132-fold
106-fold
50-fold
46-fold
SDZ concentration (mg/kg)
day 14
day 21

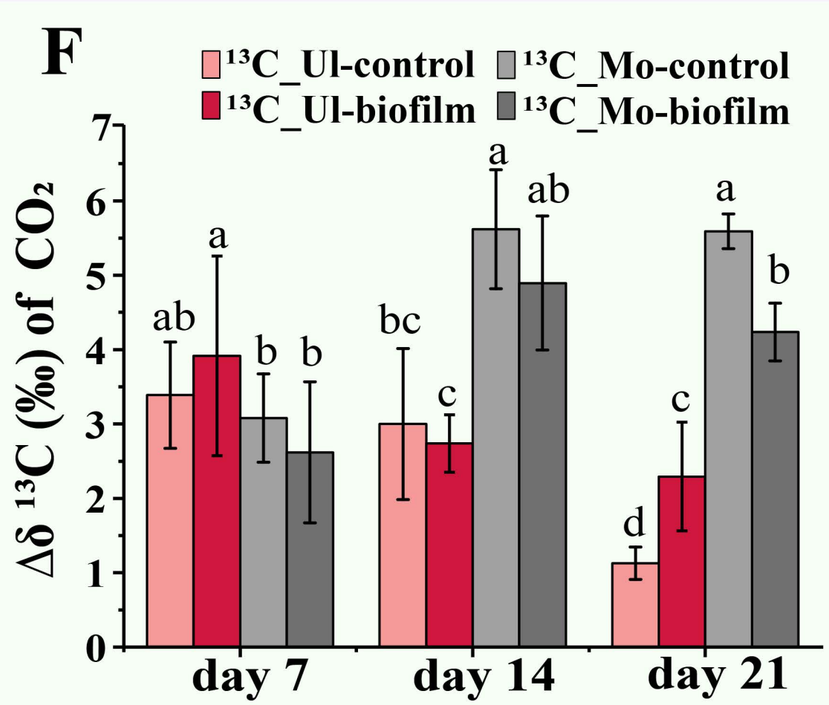
F
13C_Ul-control
13C_Ul-biofilm
13C_Mo-control
13C_Mo-biofilm
Δδ 13C (‰) of CO2
day 7
day 14
day 21

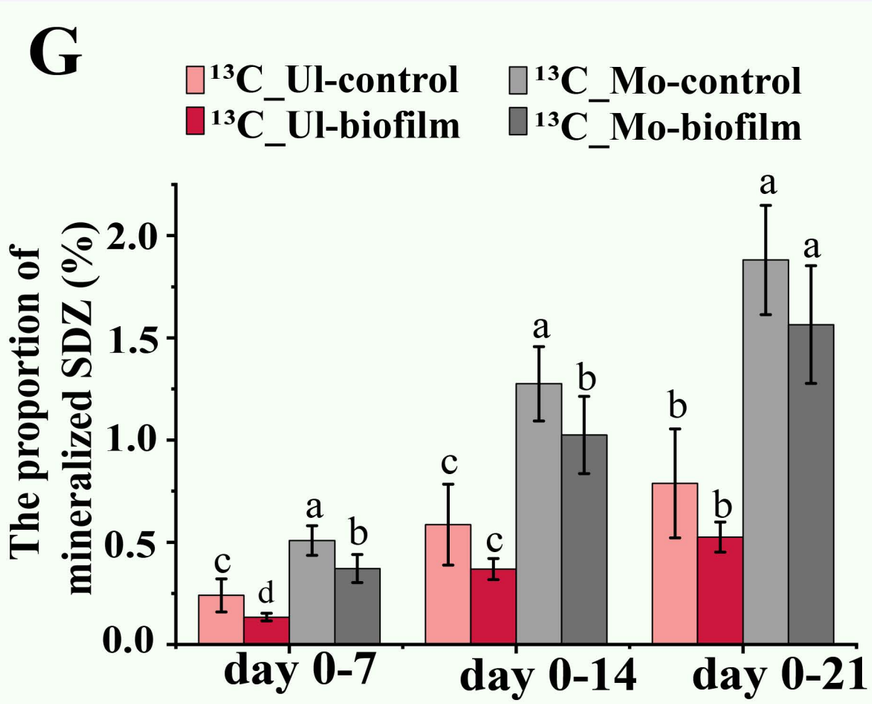
G
13C_Ul-control
13C_Ul-biofilm
13C_Mo-control
13C_Mo-biofilm
The proportion of mineralized SDZ (%)
day 0-7
day 0-14
day 0-21

A

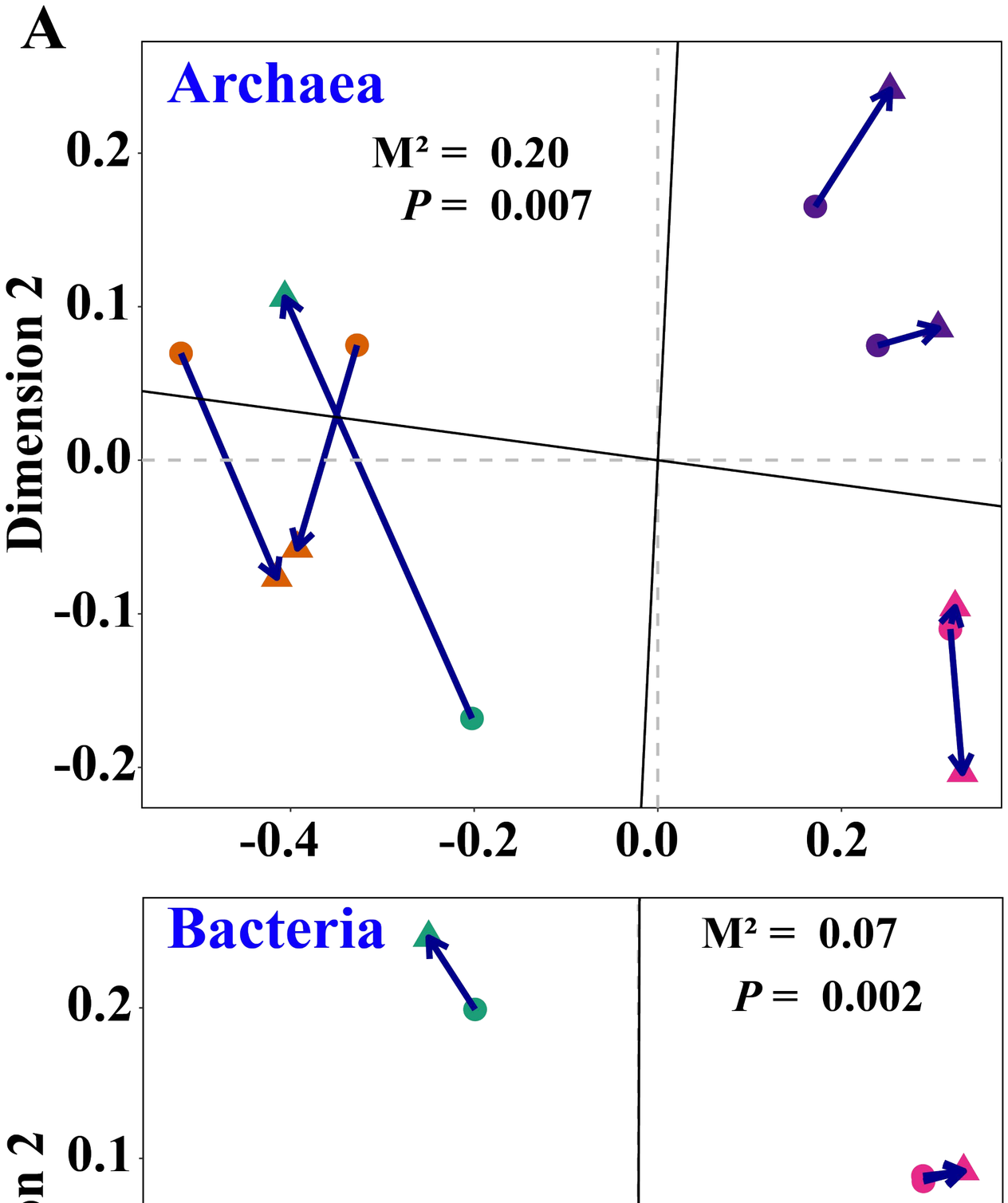

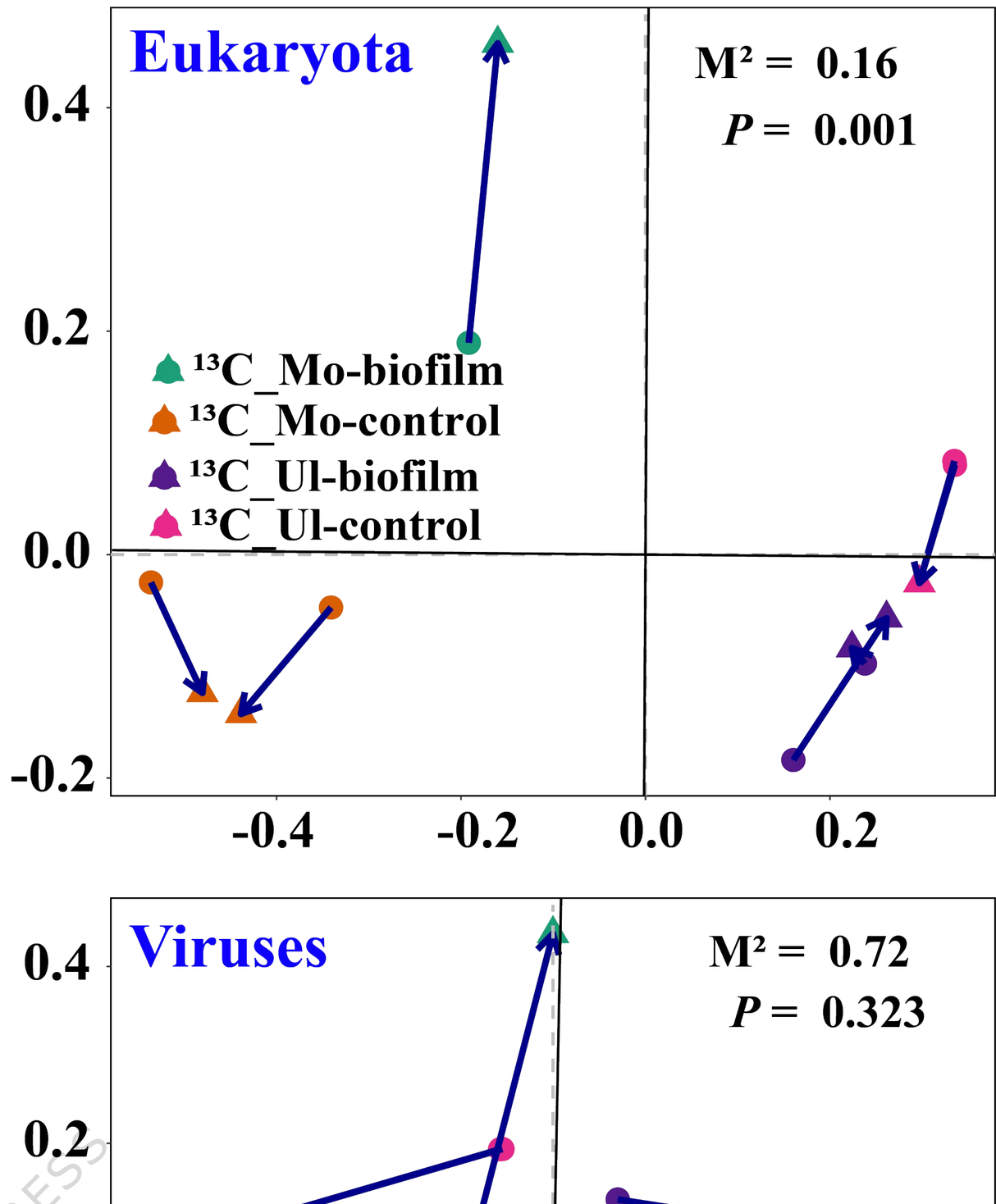

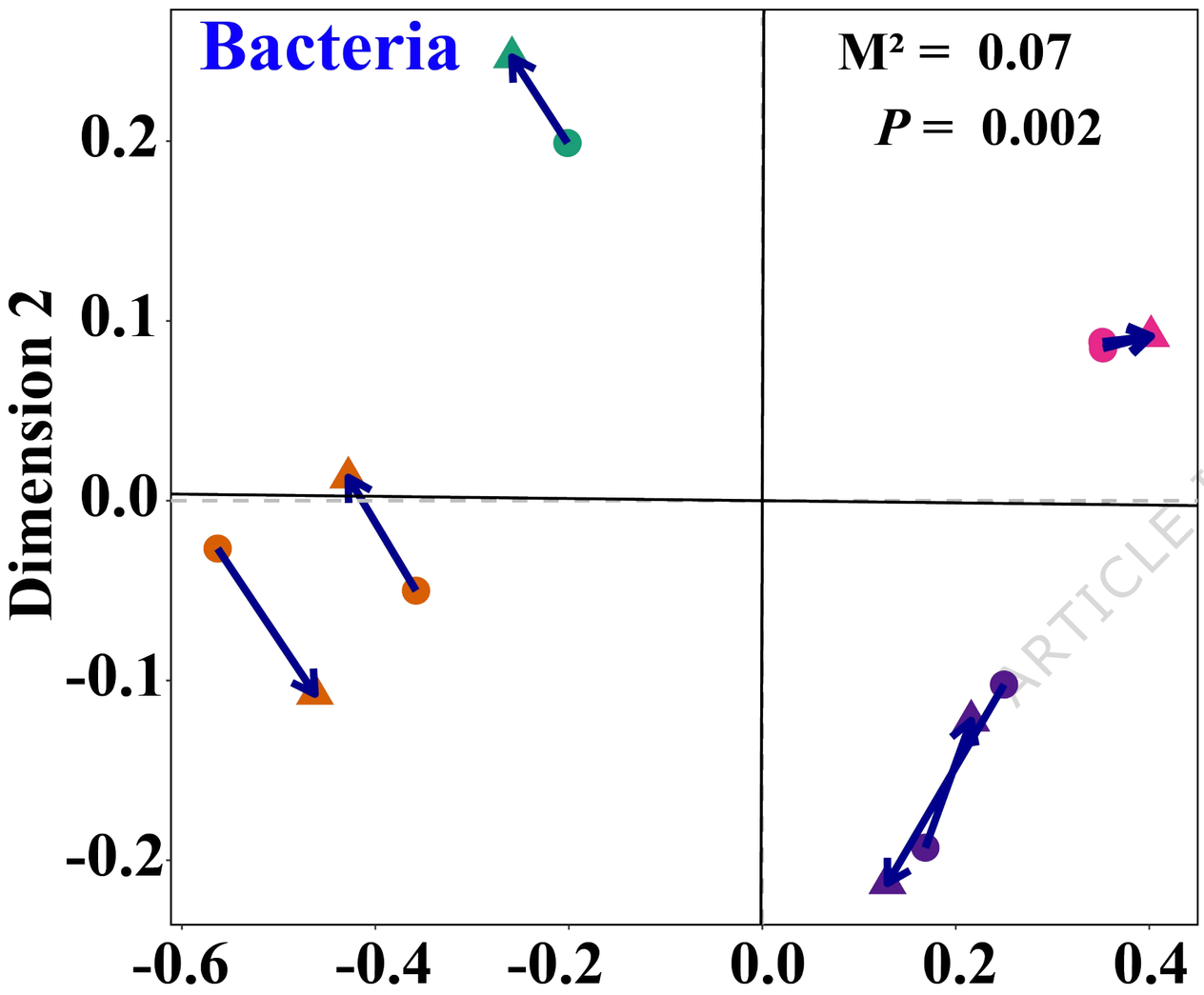

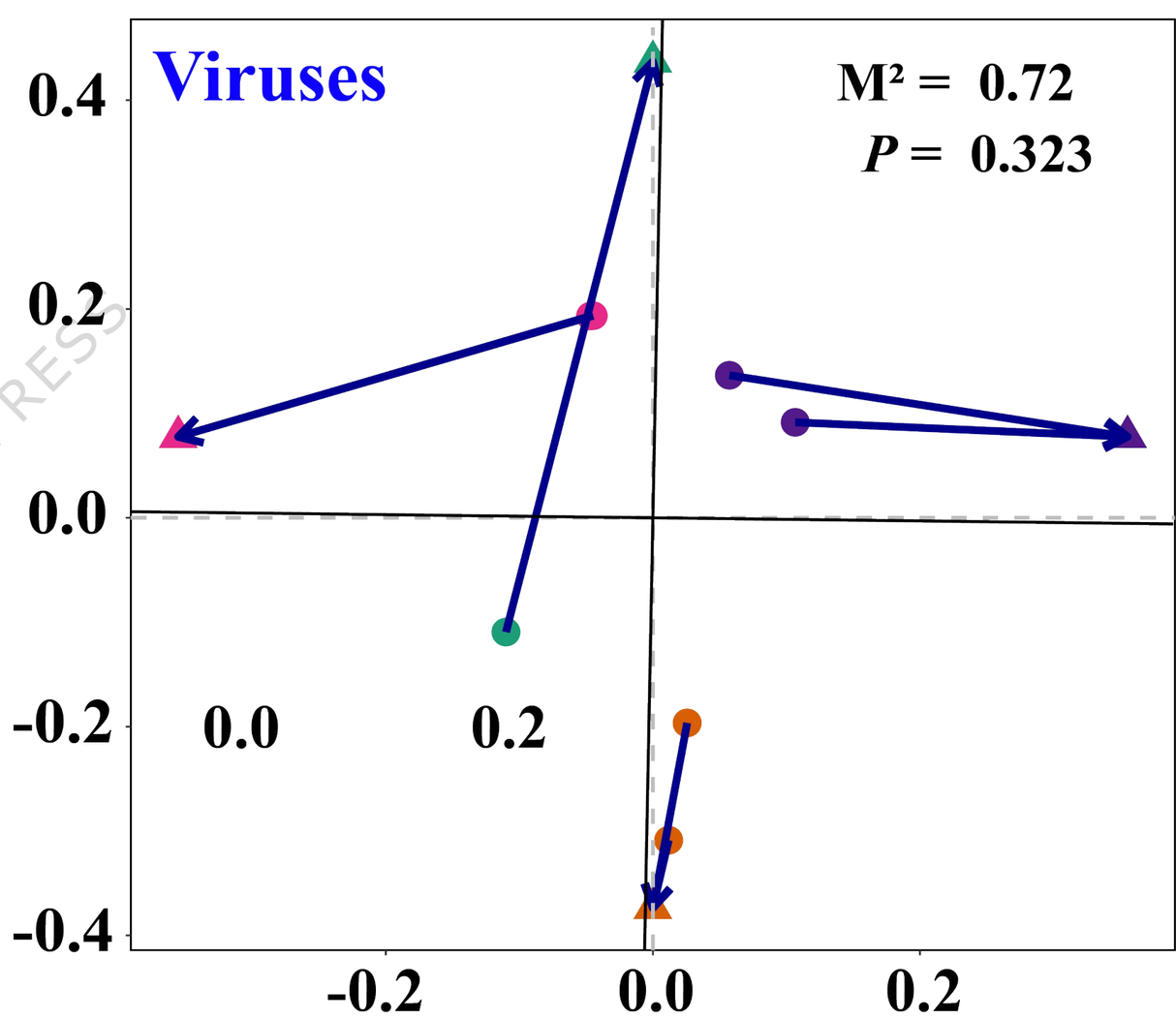

B

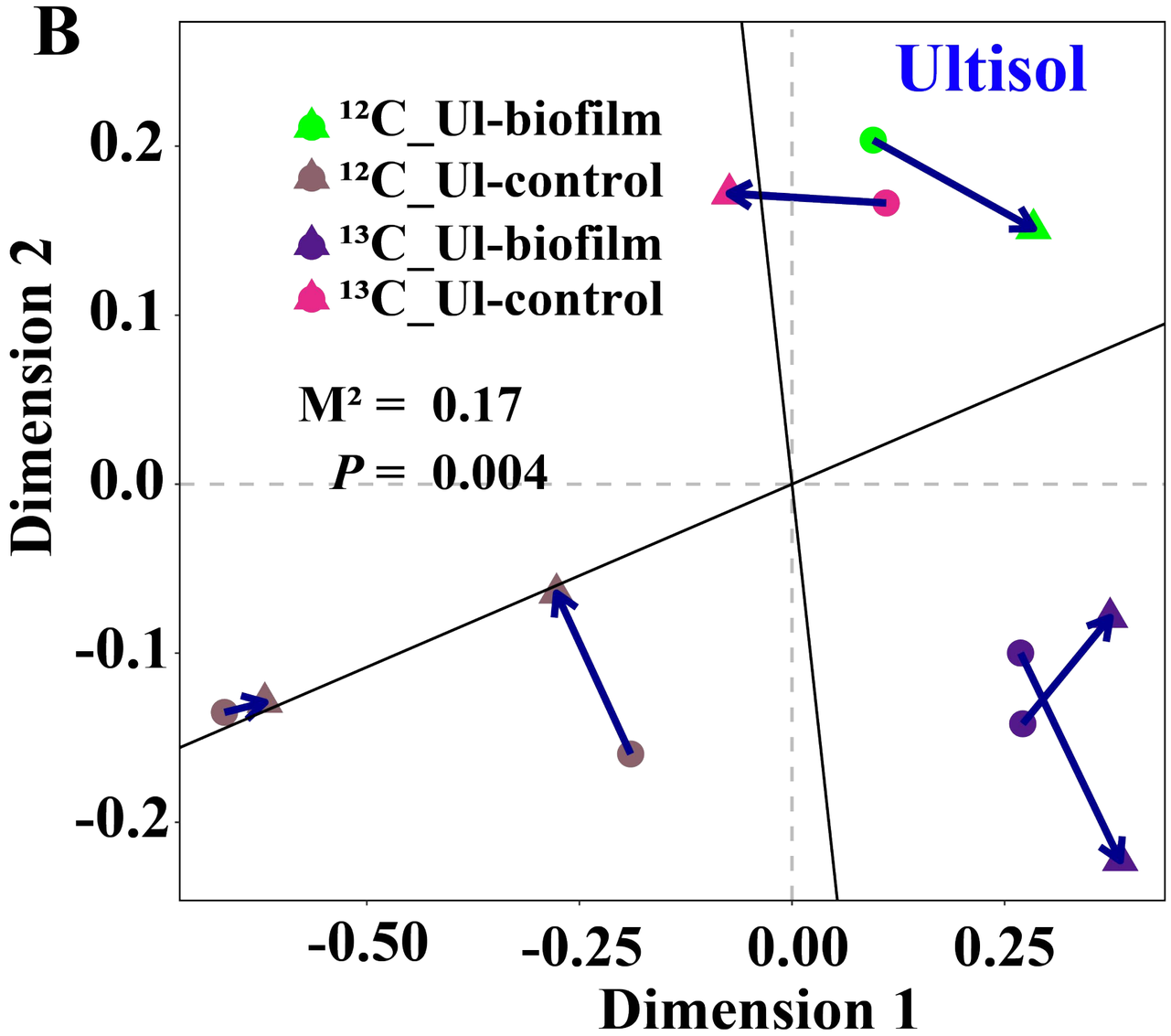

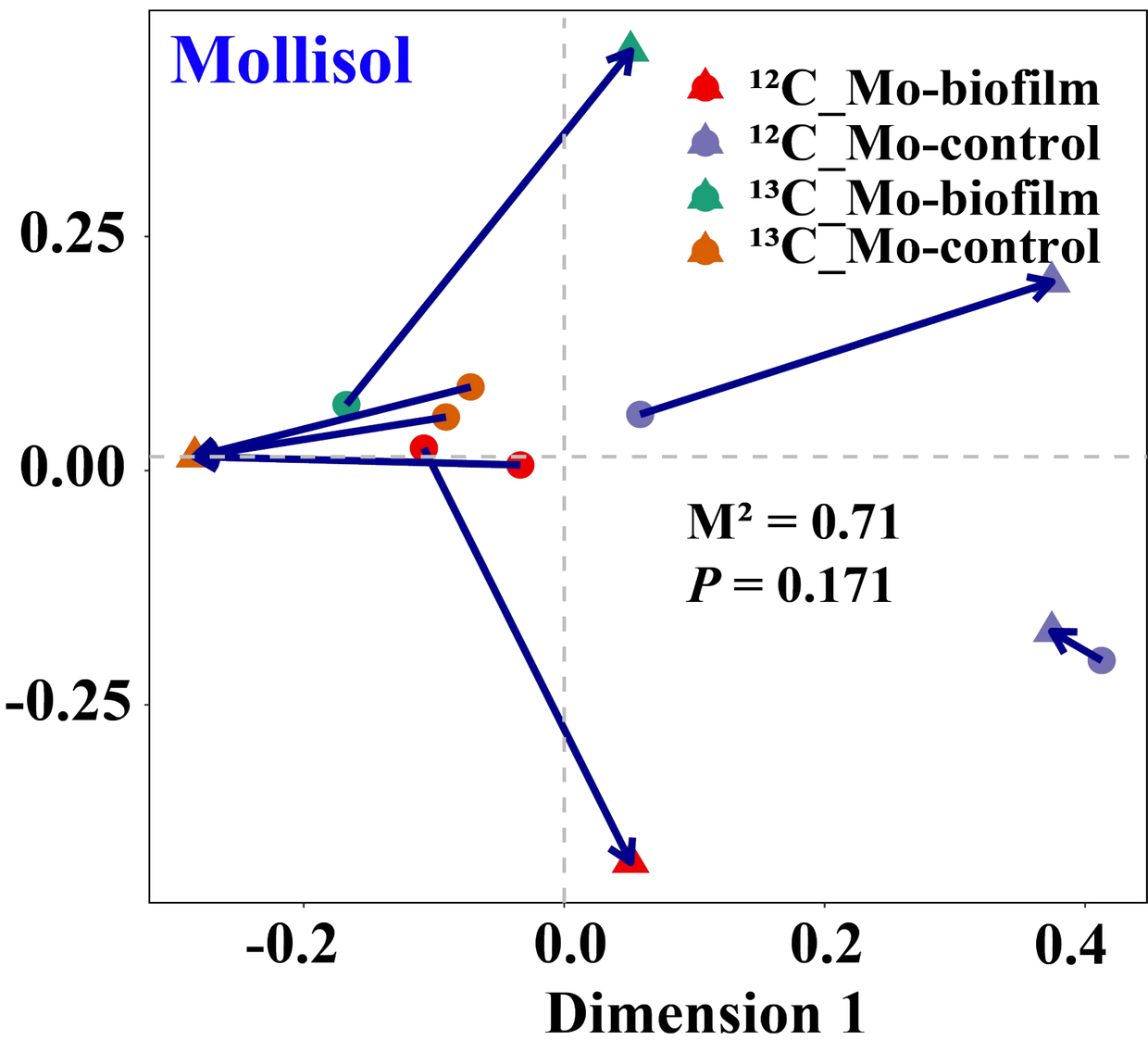

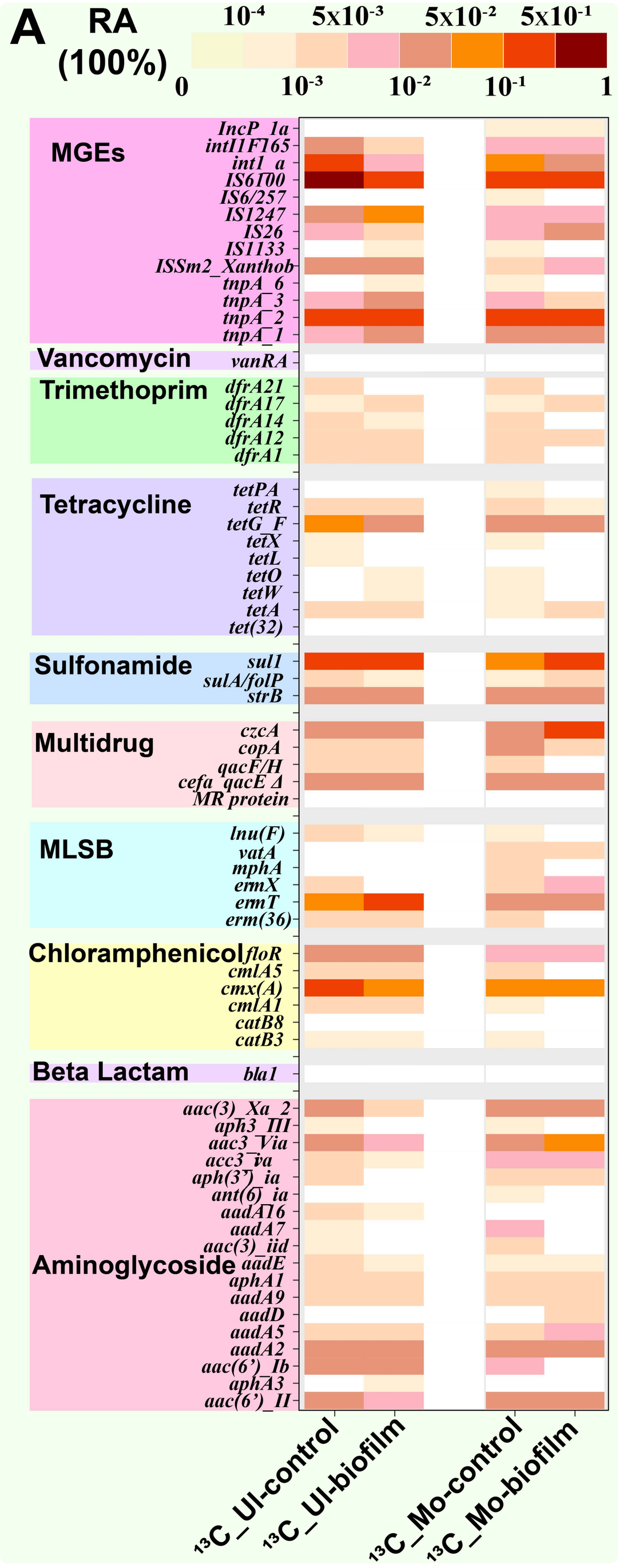
A
RA (100%)
10-4
5x10-3
5x10-2
5x10-1
0
10-3
10-2
10-1
1
MGEs
IncP_1a
intI1F165
int1_a
IS6100
IS6/257
IS1247
IS26
IS1133
ISSm2_Xanthob
tnpA_6
tnpA_3
tnpA_2
tnpA_1
Vancomycin
vanRA
Trimethoprim
dfrA21
dfrA17
dfrA14
dfrA12
dfrA1
Tetracycline
tetPA
tetR
tetG_F
tetX
tetL
tetO
tetW
tetA
tet(32)
Sulfonamide
sul1
sulA/folP
strB
Multidrug
czcA
copA
qacF/H
cefa_qacE Δ
MR protein
MLSB
lnu(F)
vatA
mphA
ermX
ermT
erm(36)
Chloramphenicol
floR
cmlA5
cmx(A)
cmlA1
catB8
catB3
Beta Lactam
bla1
Aminoglycoside
aac(3)_Xa_2
aph3_III
aac3_Via
acc3_va
aph(3'')_ia
ant(6)_ia
aadA16
aadA7
aac(3)_iid
aadE
aphA1
aadA9
aadD
aadA5
aadA2
aac(6')_Ib
aphA3
aac(6')_II
13C_UI-control
13C_UI-biofilm
13C_Mo-control
13C_Mo-biofilm

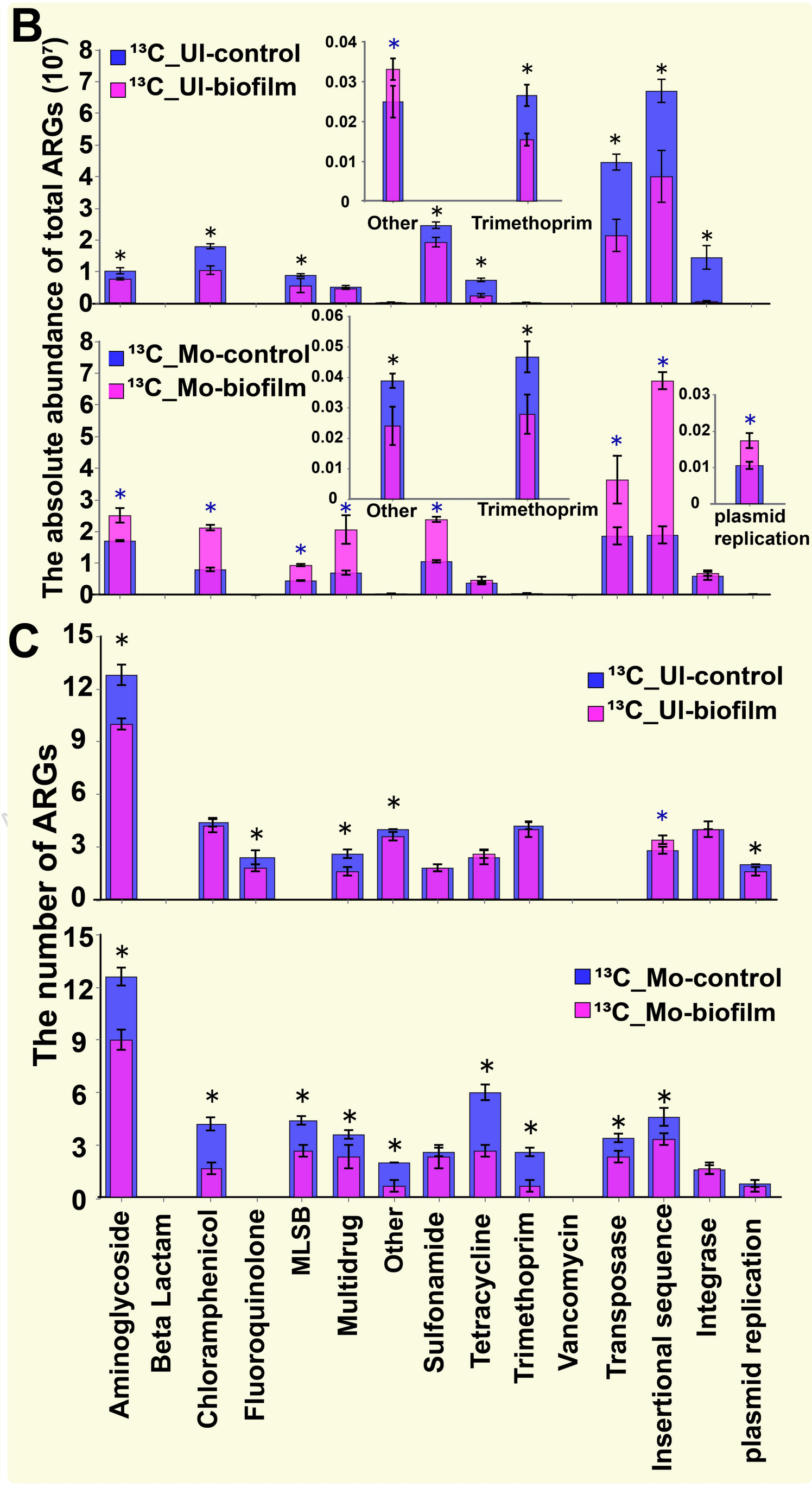
B
The absolute abundance of total ARGs (10^7)
13C_UI-control
13C_UI-biofilm
13C_Mo-control
13C_Mo-biofilm
Other
Trimethoprim
plasmid replication
C
The number of ARGs
Aminoglycoside
Beta Lactam
Chloramphenicol
Fluoroquinolone
MLSB
Multidrug
Other
Sulfonamide
Tetracycline
Trimethoprim
Vancomycin
Transposase
Insertional sequence
Integrase
plasmid replication

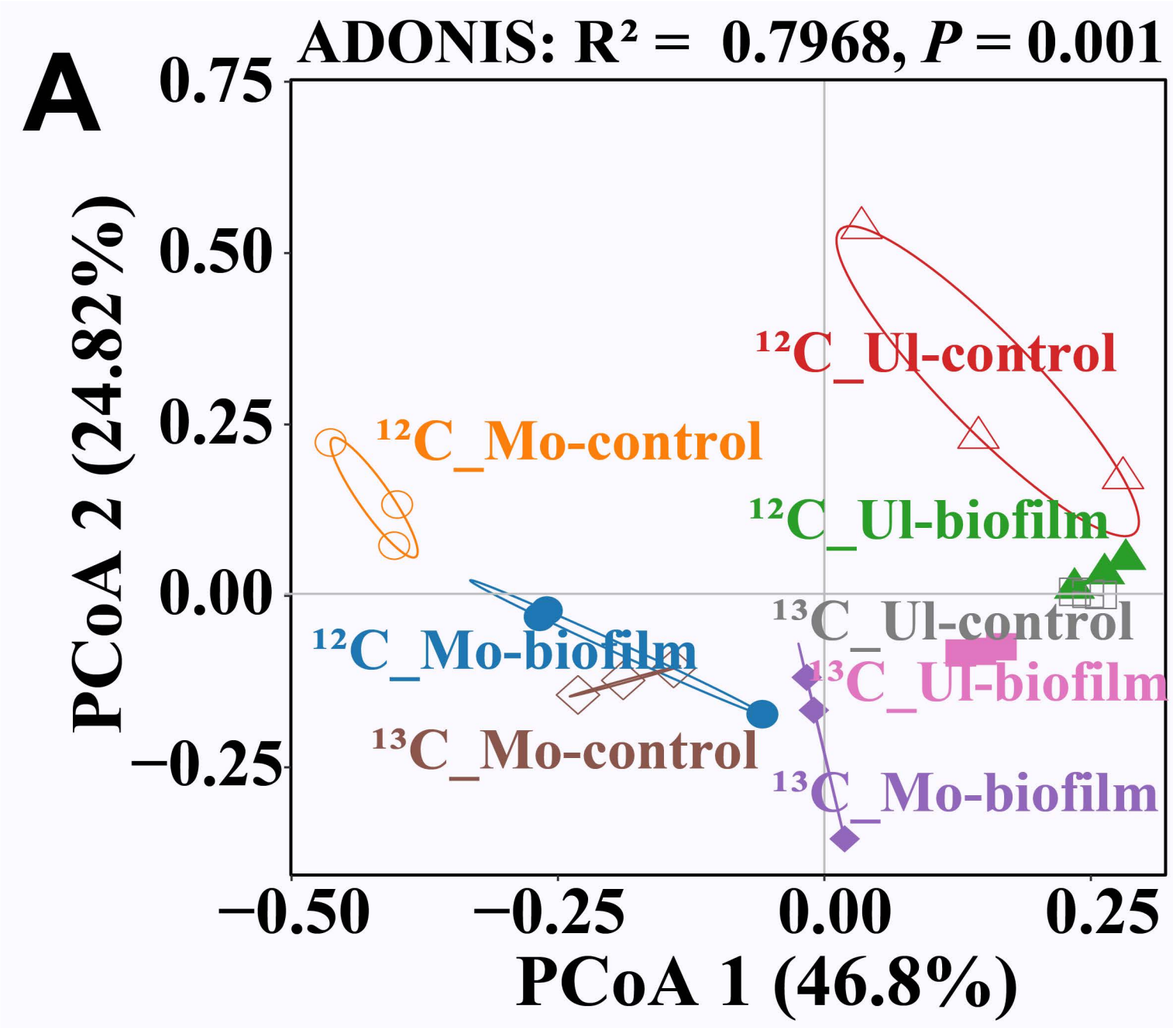
A
ADONIS: R² = 0.7968, P = 0.001
PCoA 2 (24.82%)
PCoA 1 (46.8%)
12C_Ul-control
12C_Mo-control
12C_Ul-biofilm
13C_Ul-control
13C_Ul-biofilm
12C_Mo-biofilm
13C_Mo-control
13C_Mo-biofilm

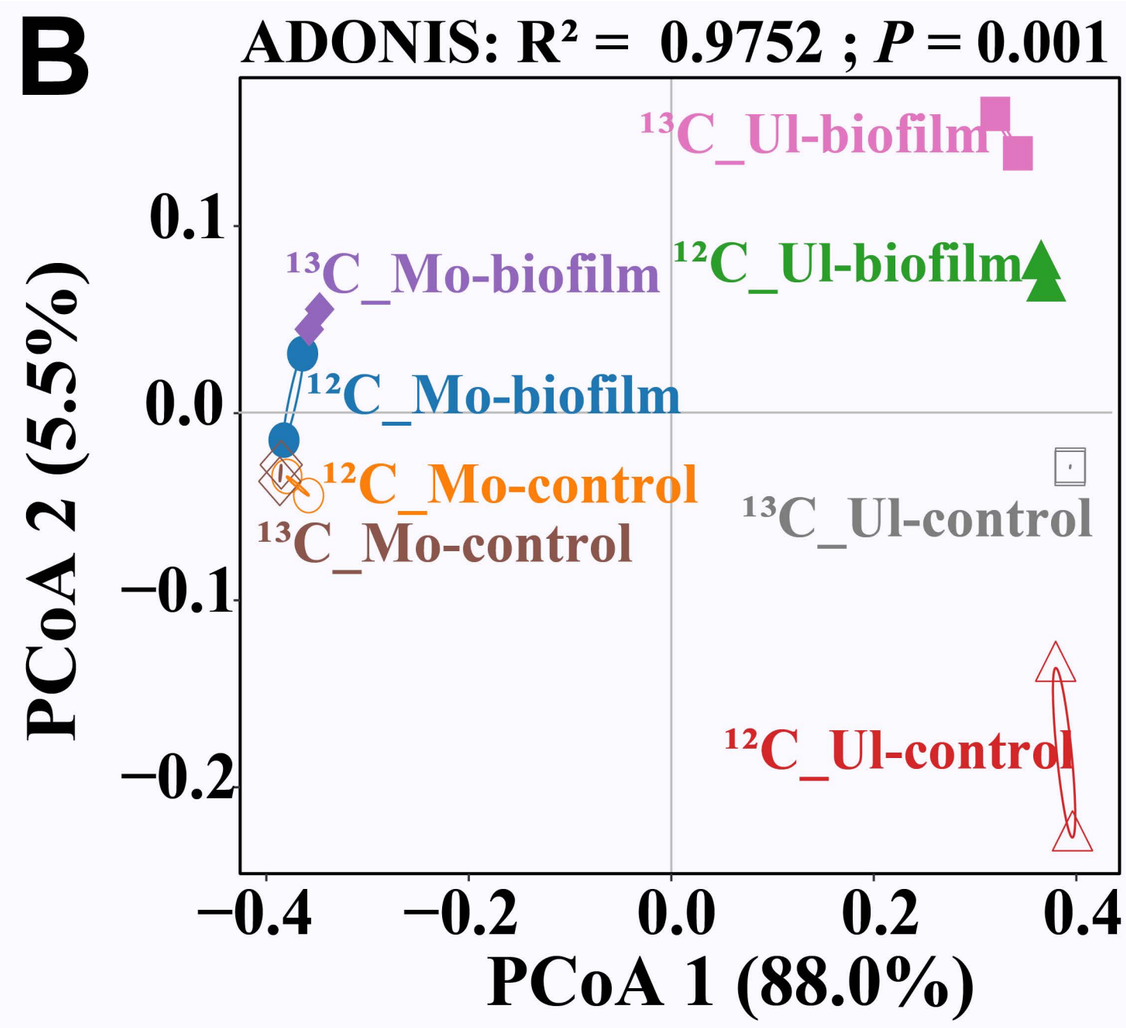
B
ADONIS: R² = 0.9752 ; P = 0.001
PCoA 2 (5.5%)
PCoA 1 (88.0%)
13C_Ul-biofilm
13C_Mo-biofilm
12C_Ul-biofilm
12C_Mo-biofilm
12C_Mo-control
13C_Mo-control
13C_Ul-control
12C_Ul-control

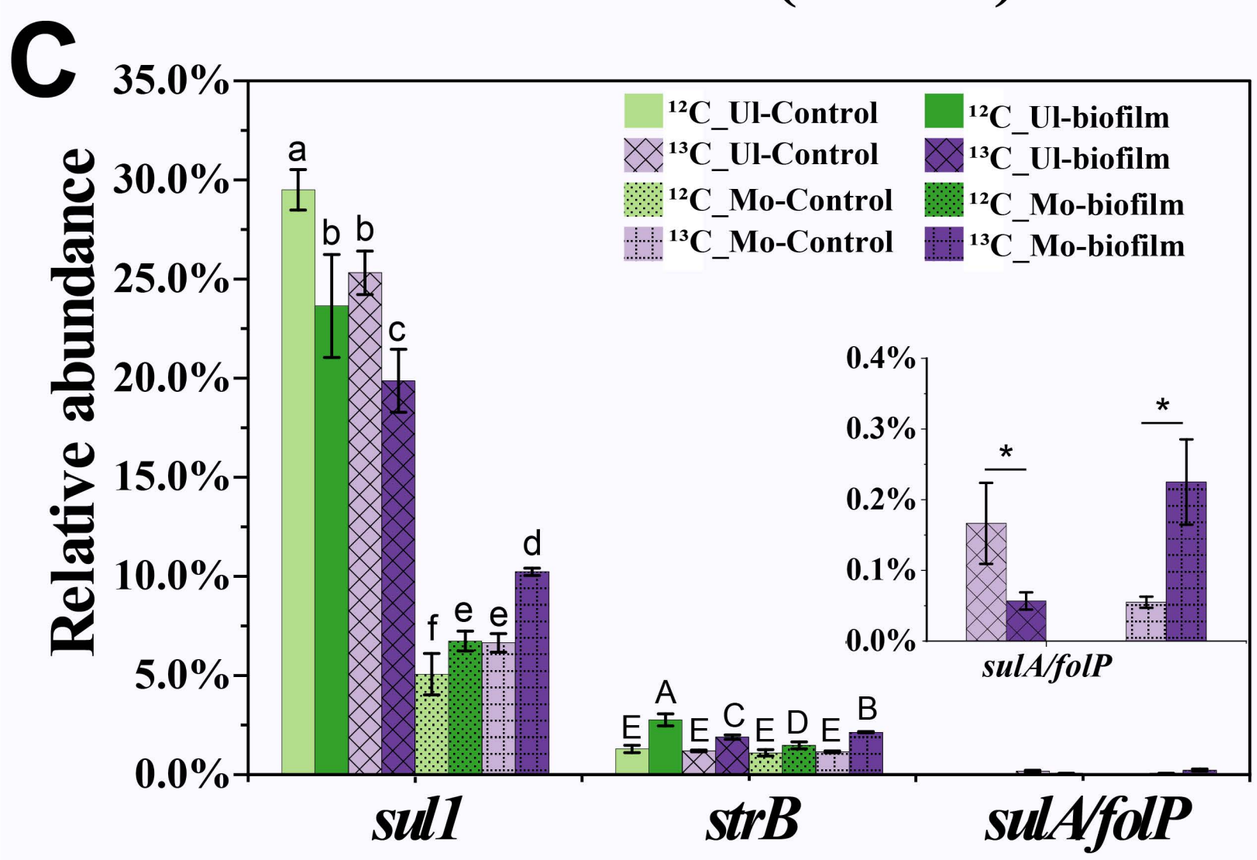
C
Relative abundance
12C_Ul-Control
13C_Ul-Control
12C_Mo-Control
13C_Mo-Control
12C_Ul-biofilm
13C_Ul-biofilm
12C_Mo-biofilm
13C_Mo-biofilm
sul1
strB
sulA/folP

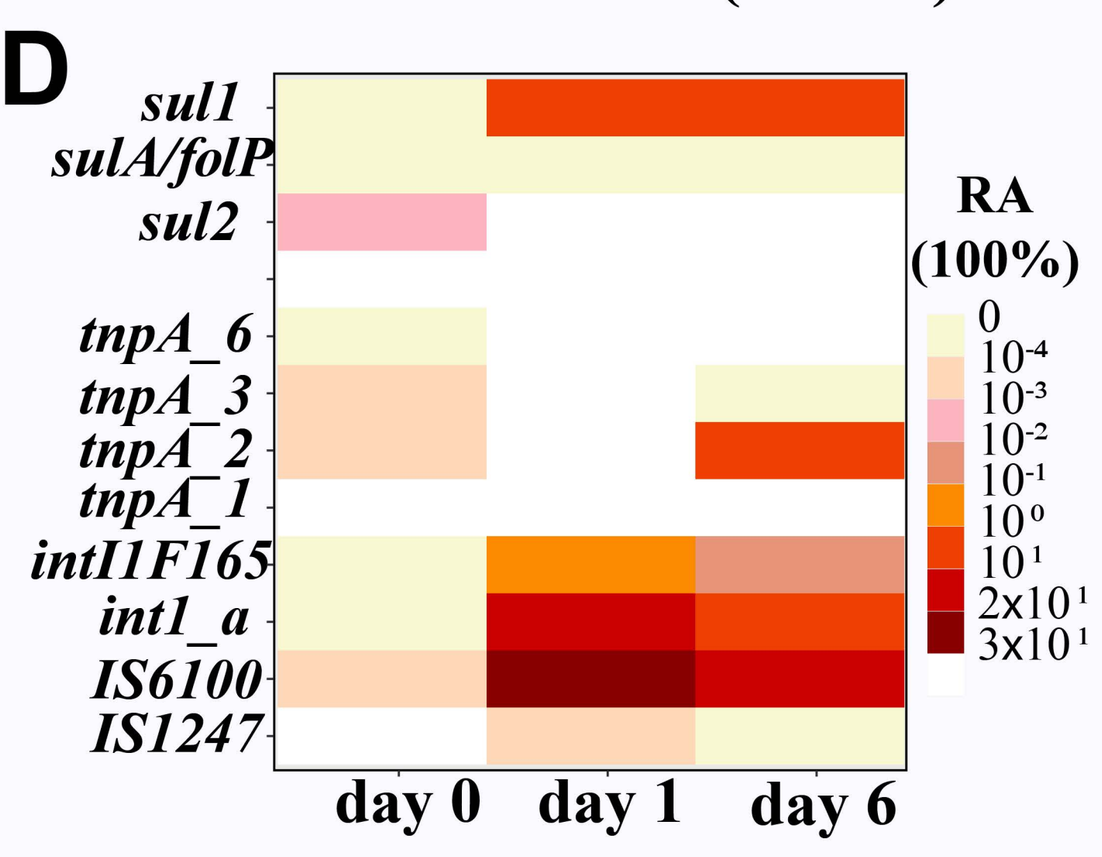
D
sul1
sulA/folP
sul2
tnpA_6
tnpA_3
tnpA_2
tnpA_1
intI1F165
int1_a
IS6100
IS1247
RA (100%)
day 0
day 1
day 6

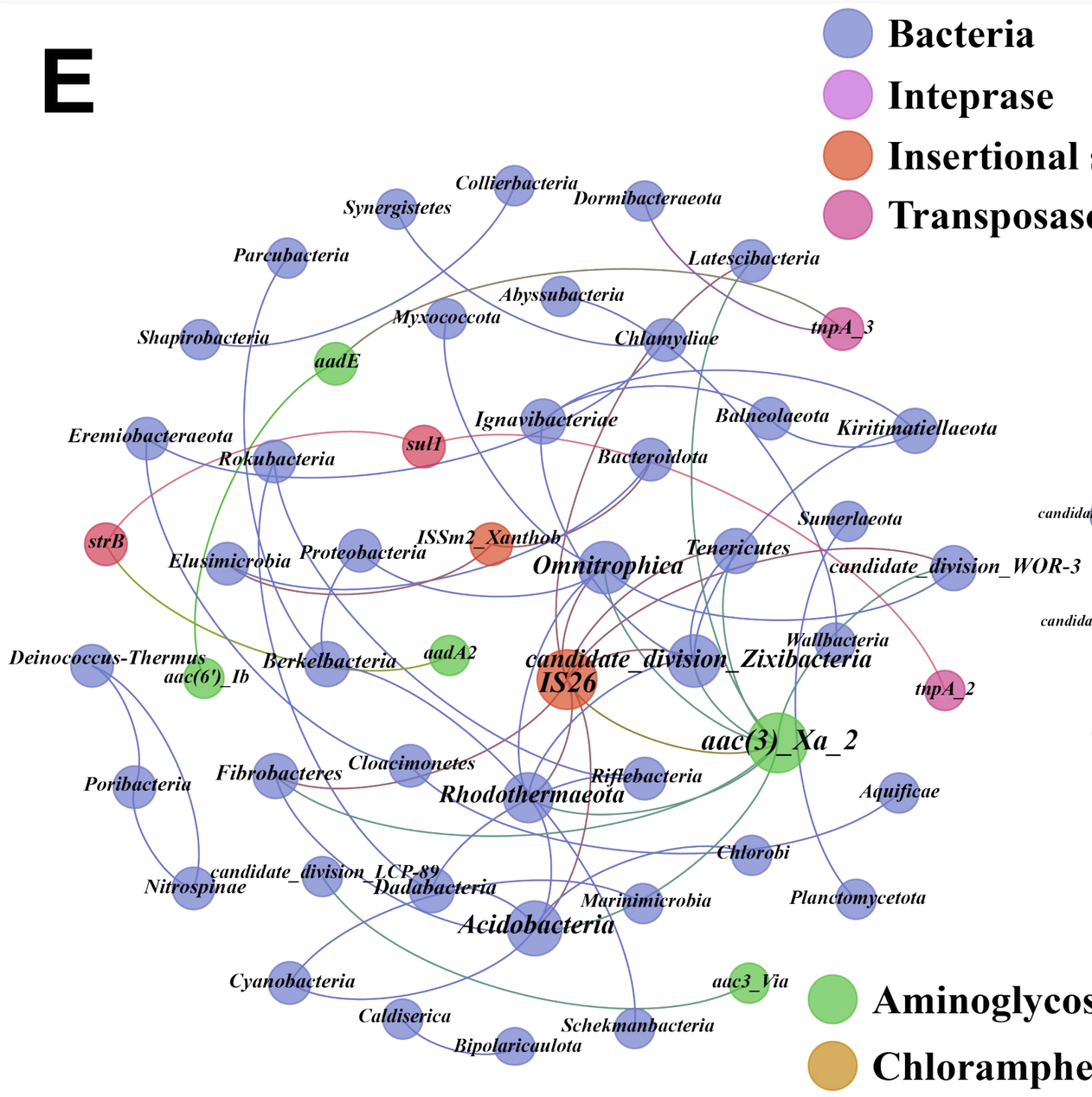
E
Bacteria
Inteprase
Insertional sequence
Transposase
Aminoglycoside
Chloramphenicol
Sulfonamide
Tetracyeline
Ultisol

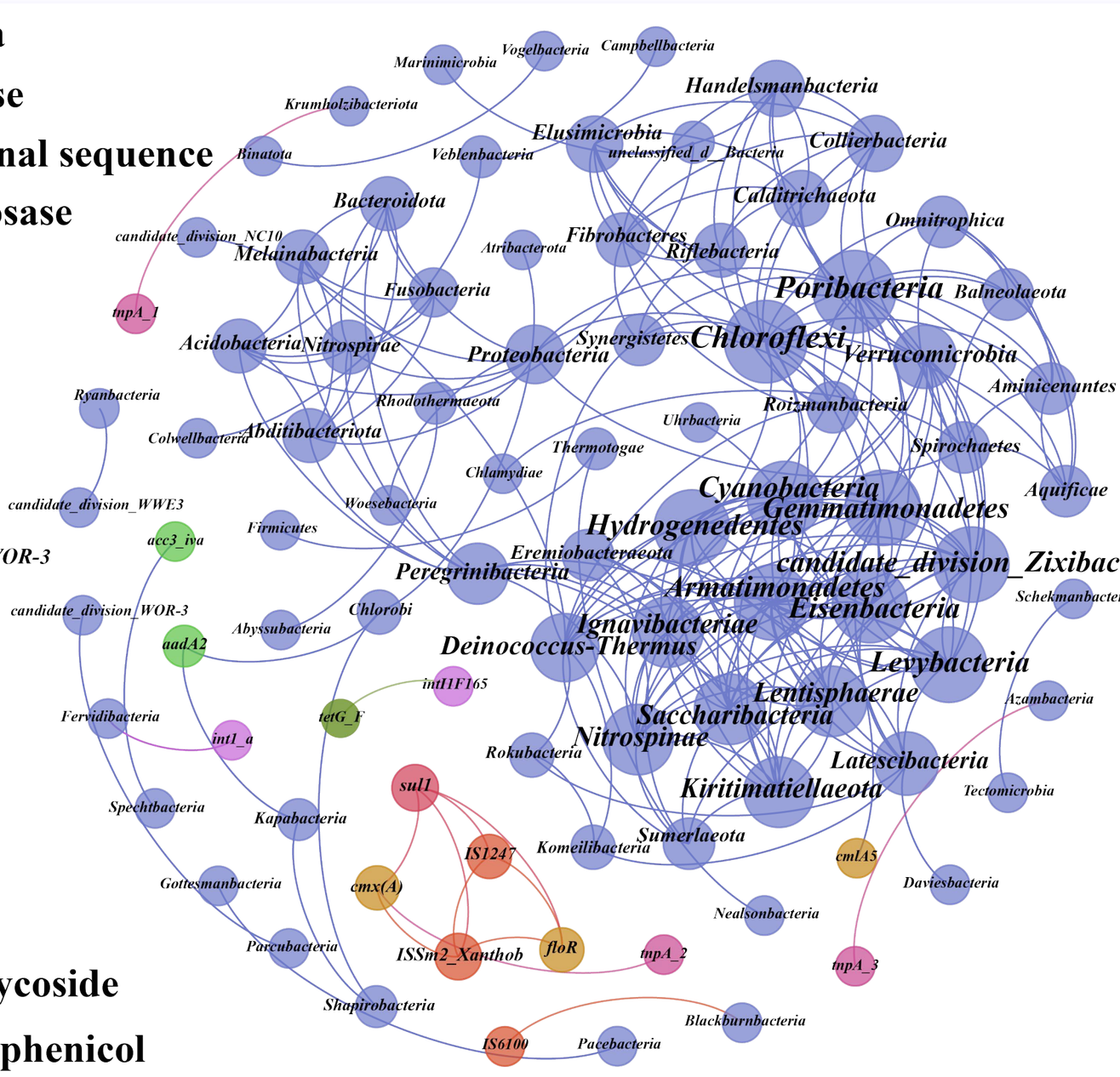
Mollisol

A

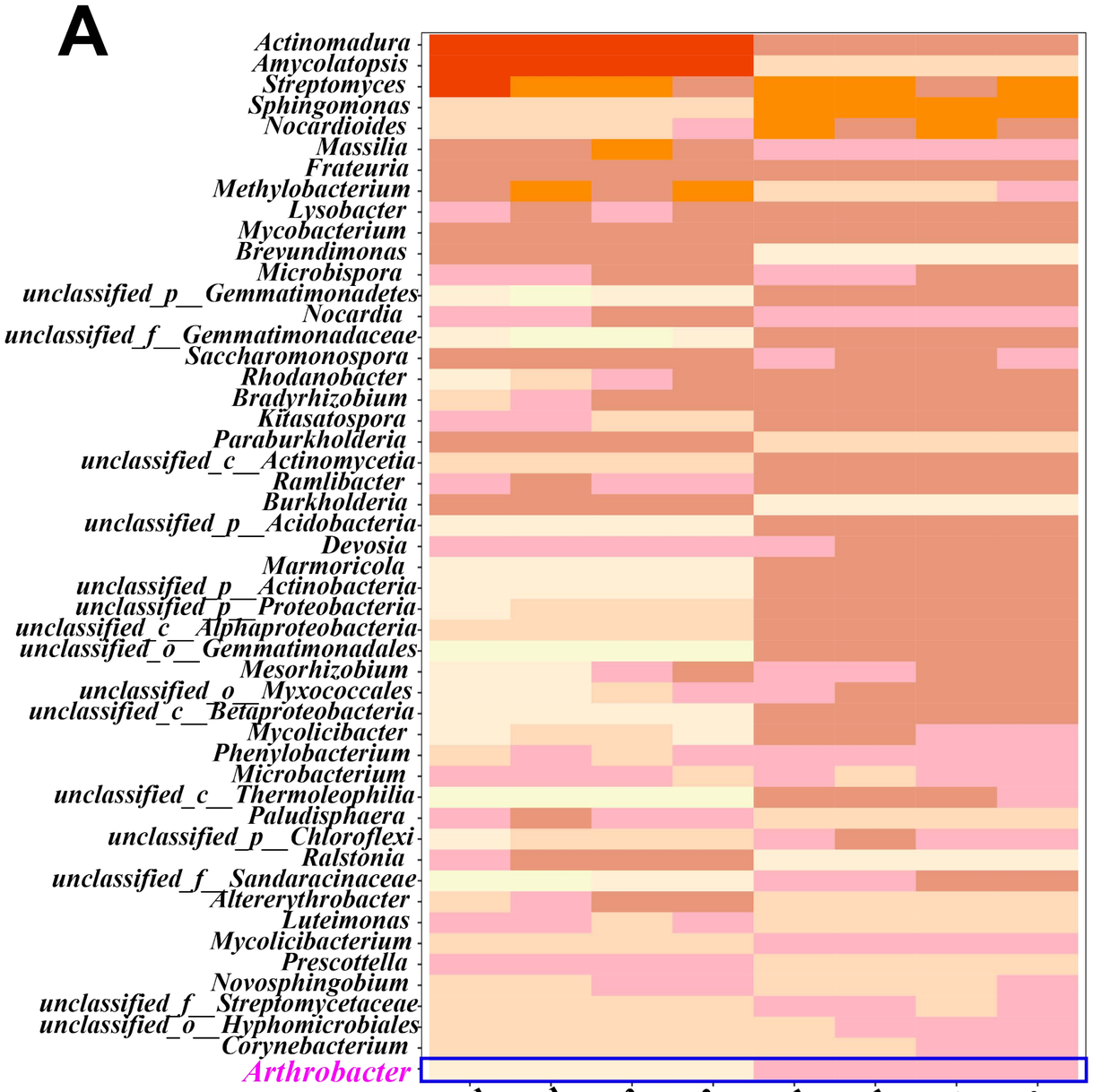

RA (100%)

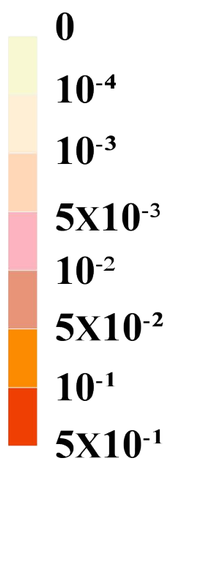

B

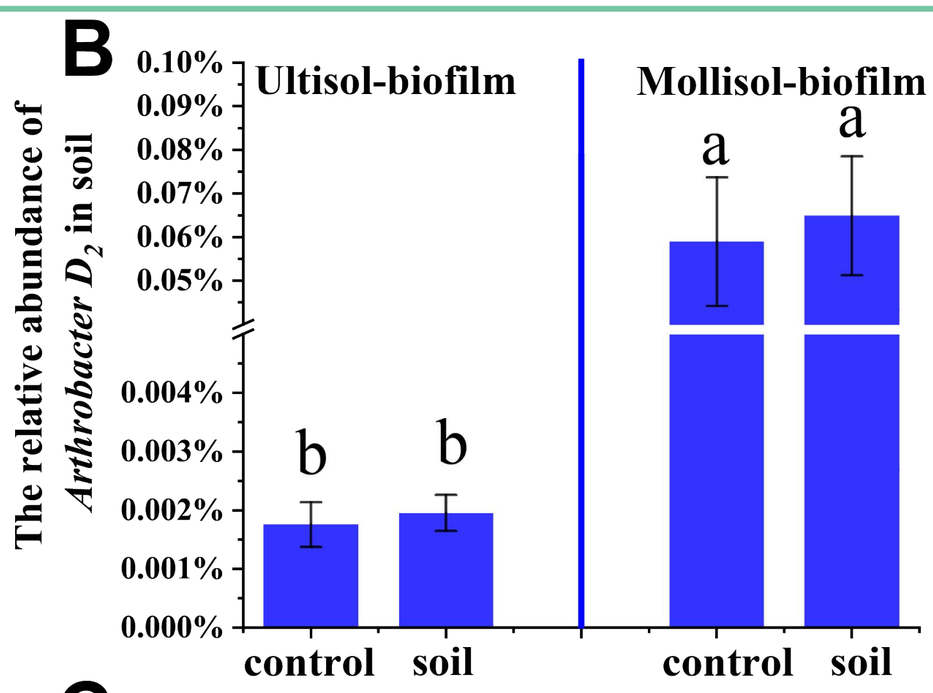

C

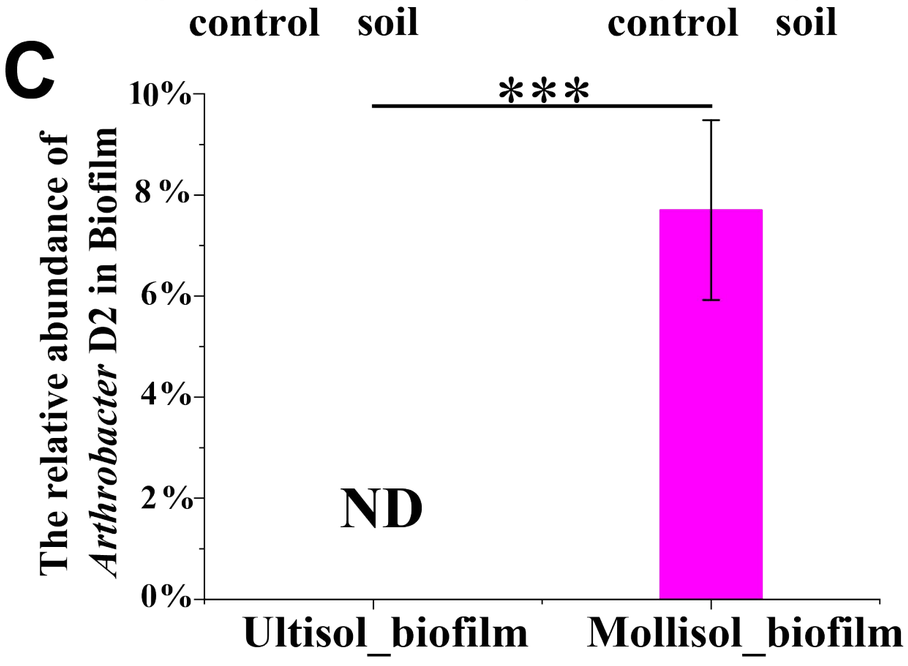

D

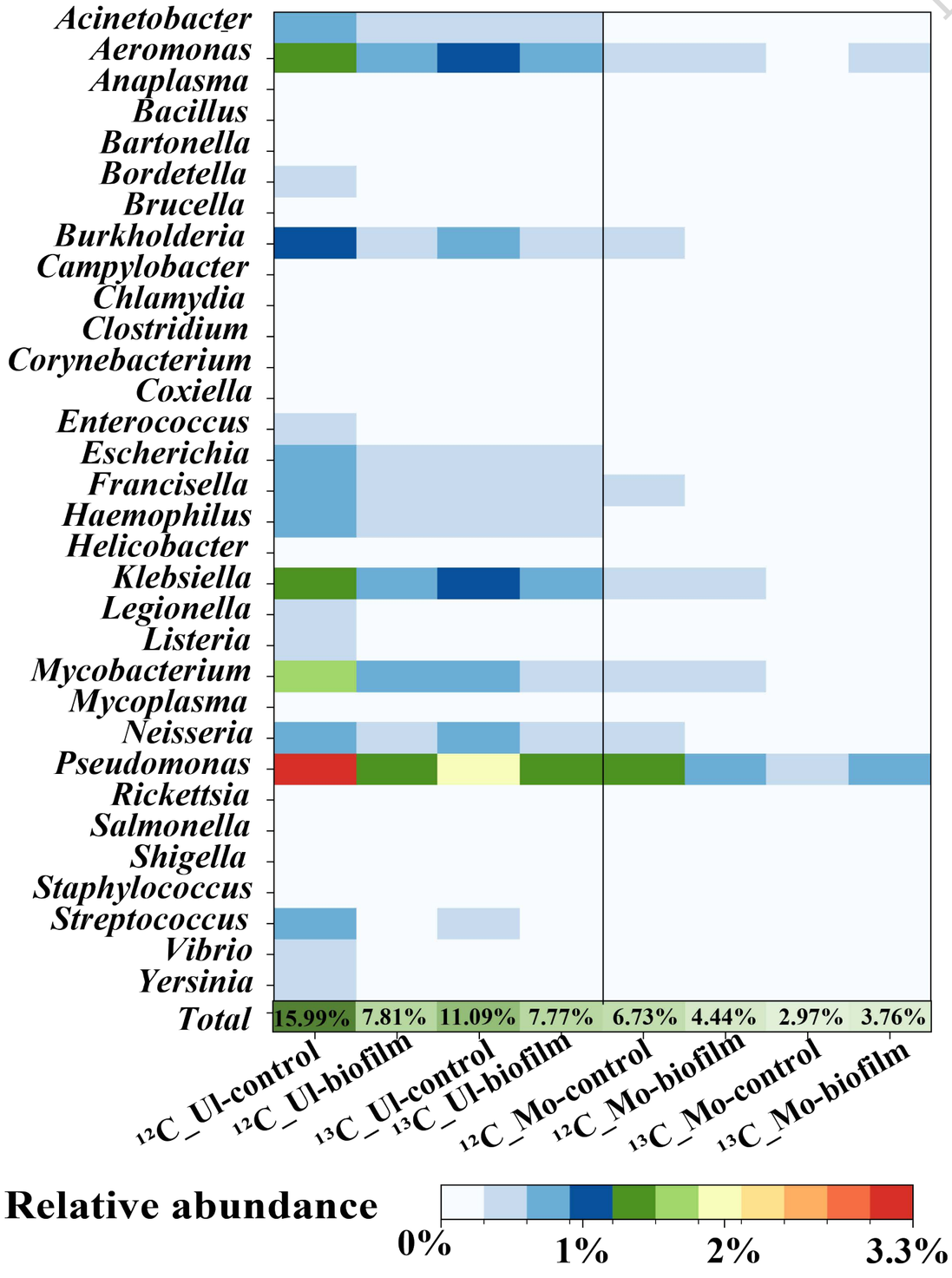

Relative abundance

E

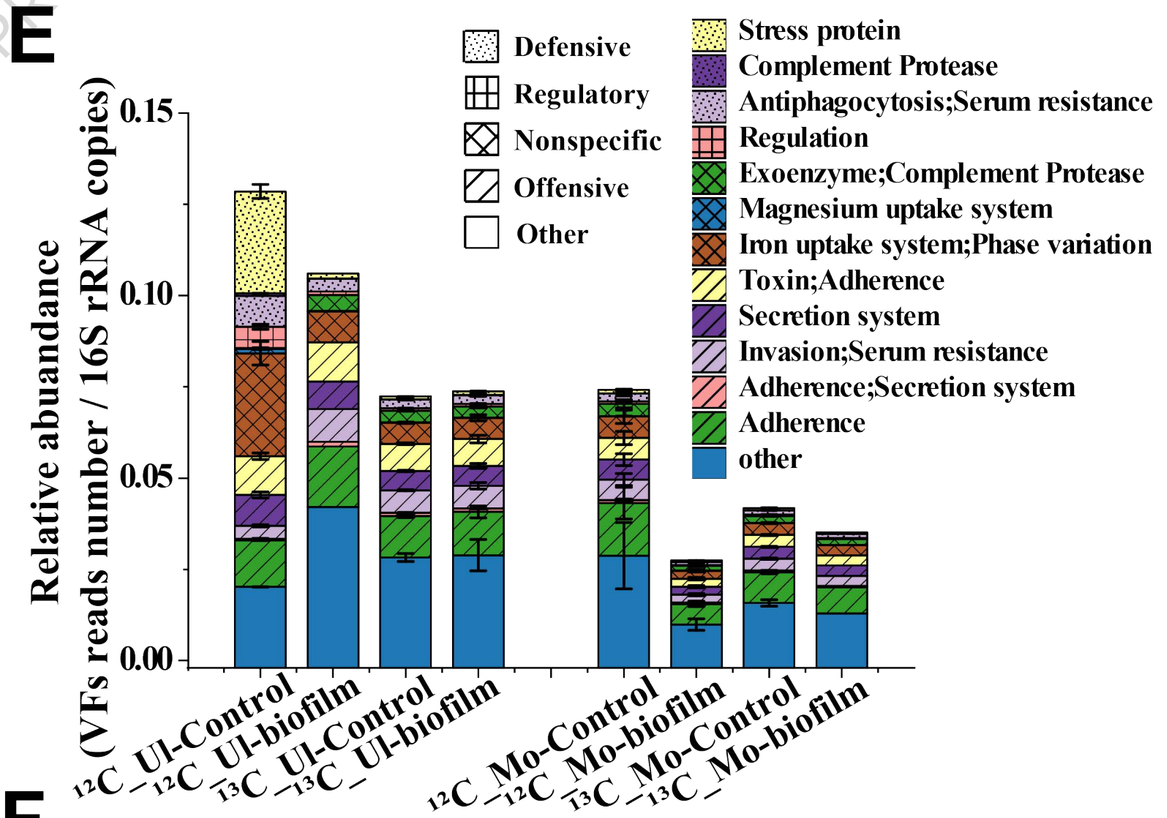

F

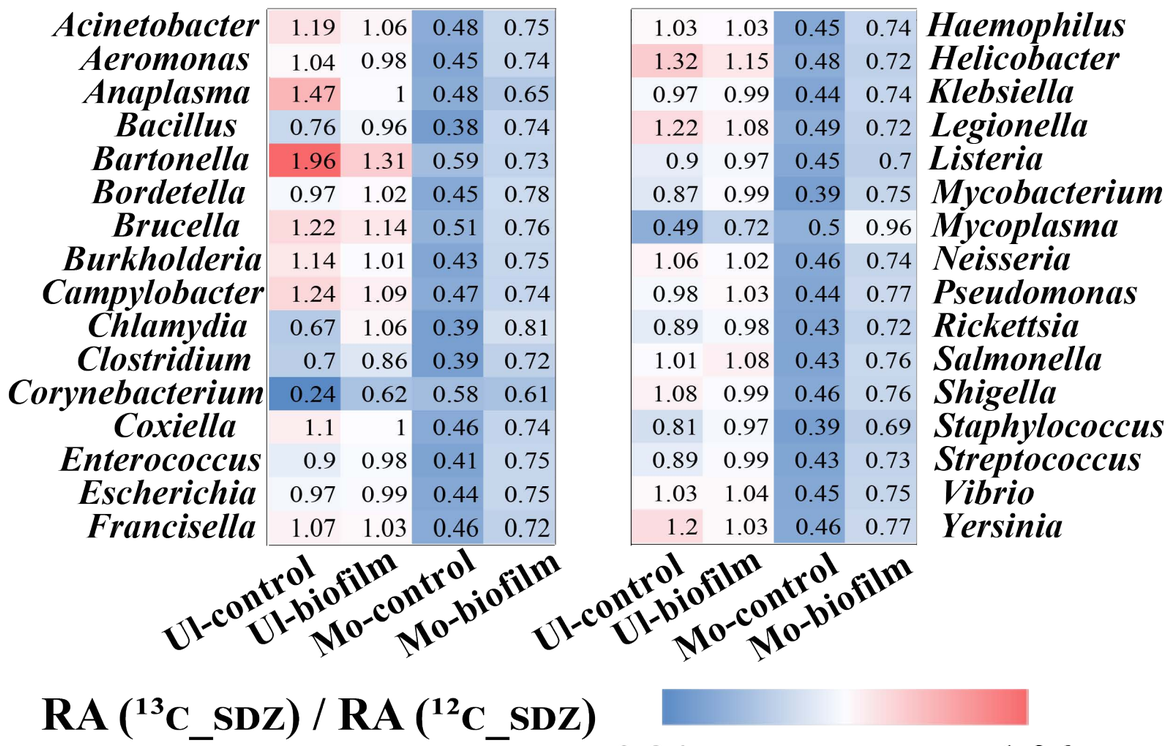

RA (13C_SDZ) / RA (12C_SDZ)